MRO Reverse Engineering Study

Assignment #1

Team 21

P. Code	Surname	Name
10724393	Chini	Filippo
10721870	Mazzitti	Riccardo
10682521	De Gennaro	Antonio
10764250	Bianco	Emanuele
10668777	Matteotti	Luca
10810285	Basci	Matteo Maria
11076681	Kazenas	Mantas

Space System Engineering and Operations

Prof: M. Lavagna

L. Bianchi, M. Bussolino

M.Sc Space Engineering
A.Y. 2024-2025

Change log	
Paragraph	*Comments*
2	pp.2: corrected and extended description of drivers
6	pp.4-5: correction of requirements
8	pp.6: addition of Interplanetary transfer description

Contents

1 High Level Goals **1**

2 Mission Drivers **1**

3 Functional Analysis **2**

4 Main Phases **3**

5 ConOps **4**

6 Level Requirements **4**

7 Scientific Instruments **5**

8 Functionalities and Phases Trajectory Design **6**

1 High Level Goals

The Mars Reconnaissance Orbiter has the purpouse of studying the Red Planet and performing several operations while orbiting Mars. In fact, during the years, MRO has served two main objectives: [8]

- Conduct scientific exploration responsive to the themes of the NASA Mars Exploration Program (MEP).
- Provide programmatic support to MEP and landed missions in terms of landing site identification for science, critical event coverage during Entry Descent and Landing (EDL), and communication relay to enhance data return.

Going into detail, the main goals of the mission are presented below with respect to the scientific phase in which they are carried out.

Preliminary Science Phase (PSP) [11-2006 to 11-2008]:

- **Aqueous activity:** Identify sites with evidence of aqueous or hydrothermal activity, which may support or preserve biological processes;
- **Geosciences:** Map and analyze the stratigraphy, geomorphology, and composition of the polar caps; improve the mapping of the Martian gravity field;
- **Present climate:** Monitor seasonal cycles and daily variations of water, dust, and carbon dioxide; study atmospheric structure, circulation, and surface interactions;

Extended Science Phase (ESP) [11-2008 to 09-2010]:

- Determine the nature and history of the Martian upper crust by focusing on crustal stratigraphy and aqueous deposits;
- Characterize ongoing surface changes studying wind-driven processes, slope changes such as gullies, and impact cratering;
- Extend the climatological record of atmospheric conditions, including weather patterns, thermal structure, dust, ice, and water vapor.

However, the ESP phase was not actually planned to keep collecting data of Mars, but to relay and support other Mars missions such as Phoenix and Mars Science Laboratory (MSL). However, the MSL launch was postponed, and so the science phase was extended. Therefore, although the functional analysis for the PSP fits well in the actually occurred ESP, drivers and requirements for the mission are only defined in the PSP.

2 Mission Drivers

Drivers are the backdrop for the entire mission and play a fundamental role in shaping the design process, the system architecture, functionalities, and performances. After an accurate analysis, the following mission drivers have been identified: [4][8]

Pointing control It is crucial to provide a precise pointing capability to acquire clear images of the planet and be able to use scientific payloads properly. This is paramount since the payloads on-board include a very high resolution camera (Hi-Rise), which requires an RPE (Relative Pointing Error) 3σ of 0.7 mrad [3]. The spacecraft must be able to orient the necessary apparatus for telecommunications and to provide the necessary power to the systems and instrumentation. To achieve that, the Attitude Determination and Control Subsystem (ADCS) is based on thrusters and reaction wheels.

Reaching Primary Science Orbit (PSO) In order to achieve the major mission goals, the spacecraft must be placed in a near-circular, near-polar, Sun-synchronous orbit. This was done to achieve a groundtrack that covers the whole Mars surface (in approximately 17 days). In order to achieve this, an aerobraking is needed to save fuel. The aerobraking phase concerns different subsystems, such as the Propulsion System, as previously stated, and the Thermal Control System, because instruments must be maintained within the survival range of temperature during the transfer and aerobraking, and this influences the trade-offs of surface materials in order to withstand high thermal loads.

Data Transfer An important aspect of the mission is to be able to transfer a high data volume and this happen over different periods of time. This is because one of the mission goals is to study Mars by taking photos of its surface and sending them to Earth. Since the volume of data is very high and the distance between Mars and Earth can be large, a High Gain Antenna was needed in order to send all the information taken from MRO to Earth.

3 Functional Analysis

References:[4][8]

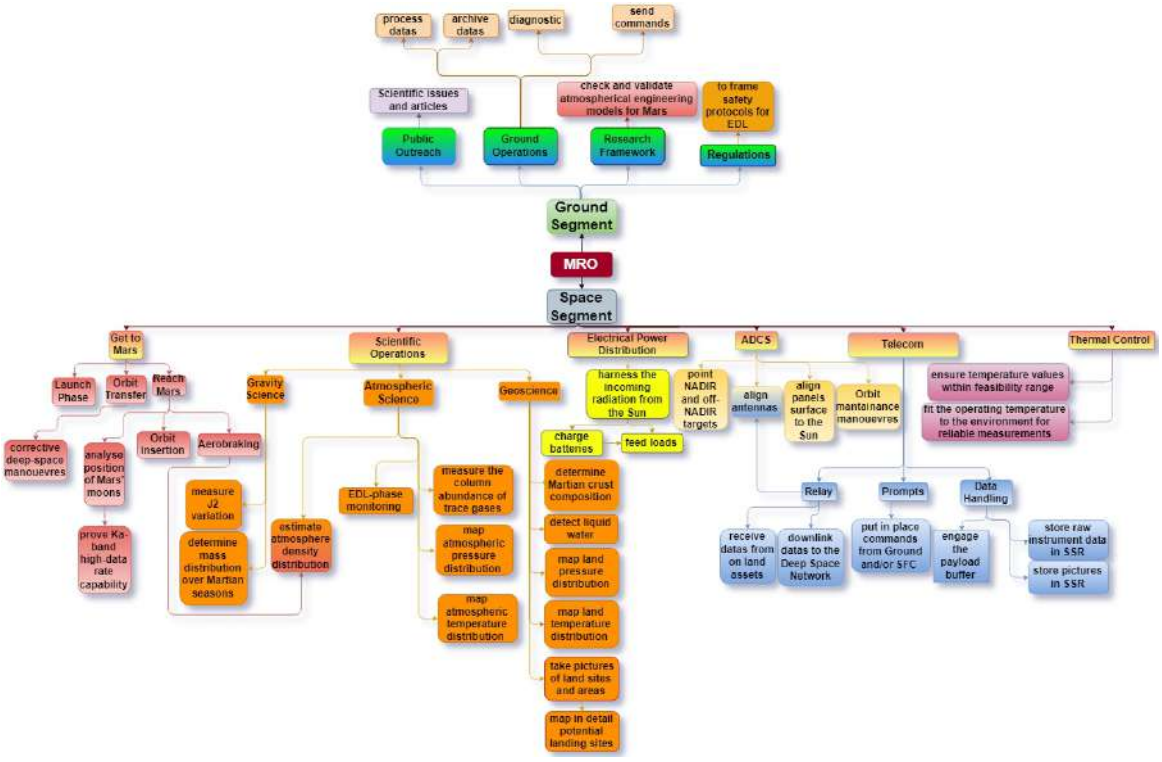

Figure 1: Functional Analysis

4 Main Phases

The MRO mission is divided in 5 main phases (references: [1] [2] [4] [5] [7]):

1. **Launch:** MRO was launched on 12 August 2005 from the Space Launch Complex 41 of Cape Canaveral, Florida at 11:43:00 GMT; the baseline launch vehicle was a Lockheed-Martin Atlas V 401, a two-stage launch vehicle. The spacecraft was delivered in a parking orbit using the Atlas booster in combination with the Centaur upper stage, and it was later placed in its interplanetary trajectory thanks to a restart of the boosters.

2. **Cruise and Approach:** This phase can be divided in two parts: the first one is the *Cruise*, which lasted five months. During this time the spacecraft followed a Type-I ballistic trajectory, as shown by Figure 2a (TCM stands for Trajectory Correction Maneuvers, that were planned to maintain an optimal trajectory). The main activities during this period of time ranged from calibrating the thrusters to in-flight check-out of the instruments and payload.
   The second part of this phase was the *Mars Approach*, which included all the preparation for a successful orbit insertion, lasted 2 months, from January to March 2006. During this phase, two more TCM were planned but they were later cancelled since the first two correction maneuvers set the orbiter on the desired trajectory.

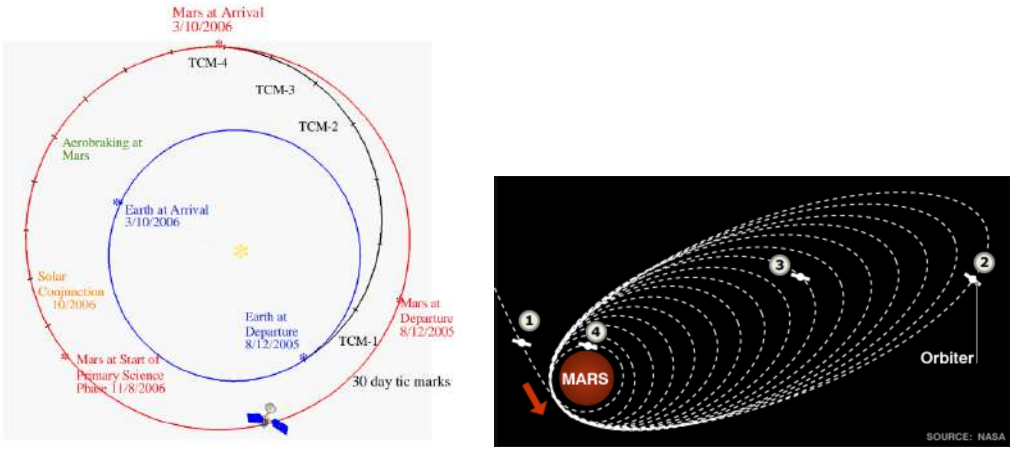

(a) Interplanetary Trajectory (b) Aerobraking Phase

Figure 2: MRO mission phases

3. **Orbit Insertion:** On 10 March 2006, by executing a propulsive maneuver that included all six main engines and lasted 27 minutes, the MRO was successfully inserted into a 35.5 h period orbit with a periapsis altitude of 425 km around Mars.

4. **Aerobraking and Transitioning:** During this phase the aerodynamic drag was used to remove kinetic energy from the spacecraft, reshaping the orbit from a highly elliptical to a near-circular, 2 h period orbit, as seen in Figure 2b. This operation began on 23 March and ended 31 August 2006, lasting for over 5 months. The Transitioning was the last phase designed to put MRO in its final science orbit; this phase lasted 2 weeks and it consisted in two propulsive maneuvers that placed the orbiter in a Sun-synchronous, near-circular orbit with periapsis (255 km of altitude) frozen over the South Pole.

5. **Primary (PSP) and Extended (ESP) Science Phases:** After completing the maneuvers to insert the orbiter in its science orbit, MRO started collecting science data, especially related

to the 3 phase overarching goals: Aqueous Activity, Geosciences and Present Climate. The PSP extended from the solar conjunction of November 2006 up to the solar conjunction of November 2008 but it was later decided, on multiple occasions, to extend the science phase because of the incredible results obtained. During this phase MRO also supported other Mars missions, such as Phoenix and MSL, providing them data for site selection.

5 ConOps

In Figure 3 the timeline of the mission is shown, including the mission phases and the operations that were planned in those phases. [6] [9]

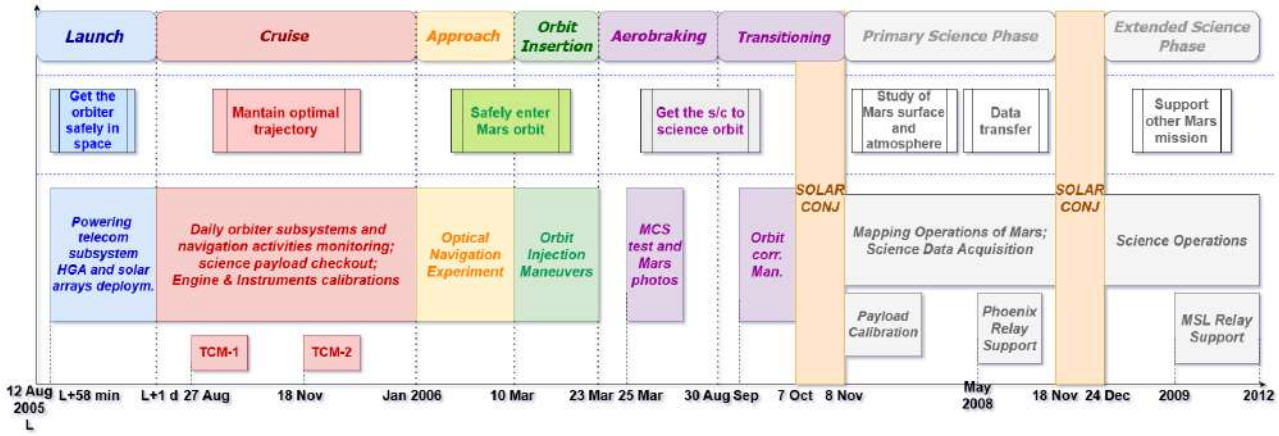

Figure 3: Correlation between ConOps, phases and functionalities

6 Level Requirements

Mission Requirements:[1][2][7]

1. **Navigation:** MRO shall achieve precise orbital transfer thanks to interplanetary insertion during launch and trajectory correction maneuvers (TCMs) during the cruise phase. The choice of a ballistic-type 1 trajectory was made to reach Mars in the shortest possible time with minimal propellant consumption.

2. **Scientific Data Acquisition:** MRO shall have capabilities to capture high-resolution images of Martian surface, study the atmosphere composition and climate dynamics over long periods of time and analyze subsurface layers in order to search for underground water or ice deposits.

3. **Relay and Support:** MRO shall have capabilities to relay data from Martian rovers on land and support missions that are reaching Mars.

System Requirements:[1][2][7]

1. **Propulsion:** MRO shall be capable to perform TCM and Aero-braking phase to arrive to Mars. MRO shall fix its orbit once every two weeks to prevent entry to Martian lower atmosphere. In order to do so the MRO Propulsion System, is composed by 12 thruster, 6 main engine and 6 less powerful, and a tank sized to accommodate 1220 kg

2. **Power systems:** To operate all the scientific and communication instruments on-board, MRO shall store a 2000 W power supplied by 20 m solar arrays supported by high capacity batteries.

3. **Communications:** For a good communication from the spacecraft to Earth and to ensure telecom link with on land assets, MRO shall use a 3 m diameter high-gain antenna, two low-gain antennas and X-band and Ka-band transmitters for high-rate data transfer.

4. **Autonomous controls and self diagnosis:** MRO shall be capable of entering into safe mode both autonomously and with commands given from Earth. It shall be able to autonomously monitor itself, determine faults and isolate/fix them.

7 Scientific Instruments

For this mission, eight scientific investigations were selected. Below is a list of the scientific payloads used and installed on this mission: [8]

1. **Compact Reconnaissance Imaging Spectrometer for Mars (CRISM)**: an advanced imaging spectrometer designed to analyze both the Martian surface and atmosphere. It measures spectral reflectance using two dedicated spectrometers, one operating in the Visible-Near Infrared (VNIR: 0.4 to 1.0 µm) range and the other in the Shortwave Infrared (SWIR: 1.0 to 3.9 µm) range. Both spectrometers can function in either a survey mode (long strips typically at 180 $\frac{\text{m}}{\text{pixel}}$), capturing broad areas, or a targeted mode for higher-resolution observations (typically at 18 $\frac{\text{m}}{\text{pixel}}$ or 36 $\frac{\text{m}}{\text{pixel}}$).

2. **High Resolution Imaging Science Experiment (HiRISE)**: a high-resolution camera capable of capturing detailed images of the Martian terrain. As its name suggests, HiRISE achieves an exceptional spatial resolution of approximately 30 $\frac{\text{cm}}{\text{pixel}}$ from an altitude of 300 km , covering a swath width of 5.4 km based on 9 panchromatic Detector Chip Assemblies (DCA), each equipped with a CCD, along with 2 additional pairs of near-IR and blue-green CCDs, allowing for a central 1.2 km-wide color swath. This capability allows for the detection of fine surface features, including potential landing sites and geological formations.

3. **Context Camera (CTX)**: It captures grayscale (black-and-white) images with a resolution of 6 $\frac{\text{m}}{\text{pixel}}$ from a typical altitude of 300 km, covering a swath width of 30 km. CTX serves as a bridge between broad regional imaging and the fine-scale details captured by HiRISE and CRISM.

4. **Mars Color Imager (MARCI)**: a wide-angle camera dedicated to daily global monitoring of Martian weather and atmospheric phenomena. It captures images in 7 spectral bands, including 2 in the ultraviolet (allowing to measure ozone) and 5 in the visible range. With a spatial resolution of approximately 1 $\frac{\text{km}}{\text{pixel}}$, MARCI provides continuous observations of dust storms, cloud formations, and seasonal atmospheric changes.

5. **Mars Climate Sounder (MCS)**: an atmospheric profiling instrument that operates in both visible and infrared wavelengths to measure the temperature, humidity, and dust content of the Martian atmosphere. It provides vertical profiles with a resolution of 5 km, covering altitudes from the surface up to approximately 80 km. This instrument is crucial for studying seasonal climate variations and atmospheric dynamics.

6. **Shallow Radar (SHARAD)**: a subsurface radar designed to probe the upper layers of the Martian crust It is a collaborative effort between NASA and ASI, with ASI providing the radar instrument, which operates in the 15–25 MHz frequency range. SHARAD searches for strong radar reflections indicative of subsurface ice or liquid water within the first few hundred meters.

The shallow radar achieves a vertical resolution of approximately 20 m and a horizontal resolution of 100 m, providing valuable insights into the geophysical properties of the Martian subsurface.

7. **Electra**: a programmable telecommunications system relay and navigation package that assists incoming spacecraft in precise navigation upon arrival at Mars. Additionally, it facilitates communication by relaying signals and data between Martian landers, rovers (via an UHF antenna) and Earth (using X-band telecommunications system).

8. **Optical Navigation Camera (ONC)**: an experimental camera tested to enhance autonomous navigation for future Mars missions. By tracking the positions of Martian moons (Phobos and Deimos) relative to background stars, ONC enabled precise determination of the orbiter's position in relation to Mars, improving orbital accuracy and navigation capabilities.

Two other scientific investigations were conducted, focusing on the study of atmospheric structure and the Martian gravitational field; these studies utilized data from onboard accelerometers and precise tracking of the spacecraft's motion to infer density variations in the atmosphere and gravitational anomalies on the surface.

8 Functionalities and Phases Trajectory Design

MRO's orbital design was carefully thought to optimize science data return, enable long-term monitoring and provide consistent data relay for surface missions. The spacecraft operates in a near-polar, sun-synchronous orbit, ensuring regular repeat observations while maintaining stability for extended operations. It is characterized by: [2] [4] [8]

- Sun-synchronous ascending node at 3 PM local mean solar time (LMST) and an inclination of 92.7°, allowing MRO to systematically observe the entire Martian surface over time. This inclination is critical for both scientific imaging and relay operations, as it allows the orbiter to pass over key regions of interest, including active rover sites and potential future landing zones, at regular intervals. The choice of a mid-afternoon LMST is optimal for the sunlight angle, which provides sufficient illumination for imaging (enhancing the signal-to-noise ratio for the various visual imaging systems) while having some shadowing to highlight the contrast topography on surface;

- an eccentricity and an argument of periapsis in a low altitude frozen orbit (periapsis altitude of 255 km and apoapsis of 320 km). In this way is possible to cross each latitude at nearly the same altitude to have essentially the same field-of-view dimensions and spatial resolutions for the instruments onboard, so it's easier to perform mapping, mosaiking and change detection;

- a semi-major axis that produce a short term groundtrack repeat cycle (semi-major axis of 3775 km with repeat cycle every 17 days). The short-term groundtrack permit any surface target to be viewed with nadir or rolled observations.

In order to achieve this type of orbit, it was performed an interplanetary Type-I ballistic trajectory from Earth to Mars. This type of transfer guarantees the minimum time to reach Mars with an optimal fuel consumption since it was essential to avoid the solar conjunction during the aerobraking phase.

References

[1] James E. Graf et al. "The Mars Reconnaissance Orbiter Mission". In: *Acta Astronautica* 57.2 (2005). Infinite Possibilities Global Realities, Selected Proceedings of the 55th International Astronautical Federation Congress, Vancouver, Canada, 4-8 October 2004, pp. 566–578. ISSN: 0094-5765. DOI: https://doi.org/10.1016/j.actaastro.2005.03.043. URL: https://www.sciencedirect.com/science/article/pii/S0094576505000780.

[2] Ben Jai et al. "An overview of mars reconnaissance orbiter mission, and operations challenges". In: *AIAA Space 2007 Conference & Exposition*. 2007, p. 6090.

[3] SW Lee and ED Skulsky. "Mars Reconnaissance Orbiter design approach for high-resolution surface imaging". In: (2003).

[4] Robert E Lock et al. "The Mars reconnaissance orbiter mission plan". In: (2004).

[5] Stacia M Long et al. "Mars Reconnaissance Orbiter aerobraking daily operations and collision avoidance". In: *Proceedings of the 20th International Symposium on Space Flight Dynamics*. 2007.

[6] Jim Taylor, Dennis K Lee, and Shervin Shambayati. "Mars reconnaissance orbiter". In: *Deep Space Communications* (2016), pp. 193–250.

[7] Tung-Han You et al. "Navigating Mars reconnaissance orbiter: Launch through primary science orbit". In: *AIAA SPACE 2007 Conference & Exposition*. 2007, p. 6093.

[8] Richard Zurek et al. "MRO overview: Sixteen years in Mars orbit". In: *Icarus* 419 (2024), p. 116102.

[9] Richard W Zurek and Suzanne E Smrekar. "An overview of the Mars Reconnaissance Orbiter (MRO) science mission". In: *Journal of Geophysical Research: Planets* 112.E5 (2007).

MRO Reverse Engineering Study

Assignment #2

Team 21

P. Code	Surname	Name
10724393	Chini	Filippo
10721870	Mazzitti	Riccardo
10682521	De Gennaro	Antonio
10764250	Bianco	Emanuele
10668777	Matteotti	Luca
10810285	Basci	Matteo Maria
11076681	Kazenas	Mantas

Space System Engineering and Operations

Prof: M. Lavagna

L. Bianchi, M. Bussolino

M.Sc Space Engineering
A.Y. 2024-2025

Change log	
Issue	*Comments*
1	First release

Contents

1 Mission Analysis **2**
1.1 Mission trajectory . . . 2
1.2 Station keeping . . . 3
1.3 Cost breakdown . . . 3

2 Propulsion system **4**
2.1 TCS Phases and functionalities . . . 4
2.2 Tank and Feeding System . . . 5
2.3 Thrusters configuration . . . 6
2.4 Reverse Sizing . . . 6
2.4.1 Propellant tank volume . . . 7
2.4.2 Pressurant tank volume . . . 7
2.4.3 Tank sizing and mass budget . . . 8
2.4.4 Power Budget . . . 8
2.4.5 Conclusions . . . 8

List of Figures

1 Pork-chop plot . . . 2
2 MRO tanks configuration: pressurant tank (white) and propellant tank (red) . . . 5
3 Propulsion System Schematics (made by the team) . . . 5
4 MRO thrusters configuration [8] . . . 6

List of Acronyms	
Acronym	*Full Name*
PSO	Primary Science Orbit
TCM	Trajectory Correction Maneuvers
MOI	Mars Orbit Insertion
OA	Orbit Adjustment
IA	Inclination Adjustment
LQ-MPC	Linear Quadratic Model Predictive Control
ACS	Attitude Control System

1 Mission Analysis

1.1 Mission trajectory

The mission has different phases in which it performs different maneuvers to accomplish the PSO orbit. Basing the studies on the original design, those phases can be divided in:

- **Launch**: the spacecraft has to reach Mars as soon as possible since it shall avoid the solar conjunction before his arrival, and also the Δv budget has to be saved. To do so, it shall be chosen a compromise between cost and time of arrival to Mars. In Figure 1 is reported the pork-chop plot for the Earth to Mars travel with the boundaries of launch and arrival window;

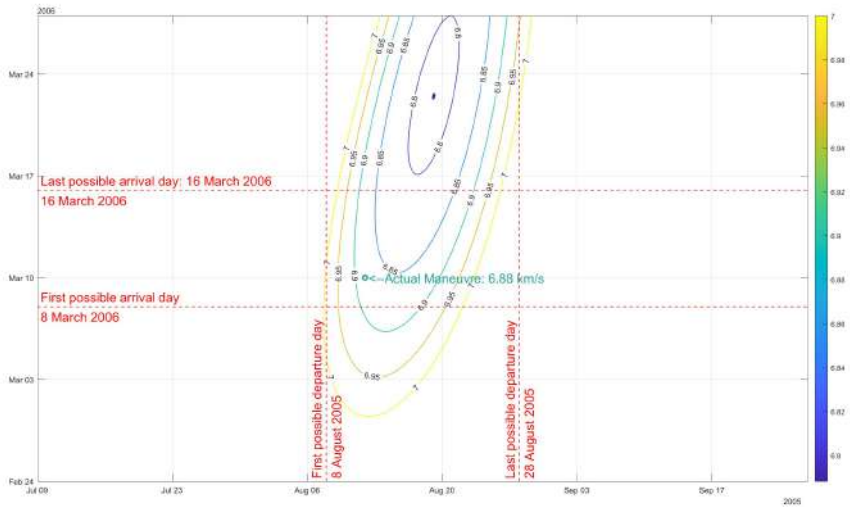

Figure 1: Pork-chop plot

- **Cruise**: to tune the pericenter altitude of the hyperbola on Mars, during the cruise shall be performed some trajectory correction maneuvers (TCMs) which cost is in the order of 1 to 8 $\frac{\text{m}}{\text{s}}$ each [8];
- **Mars Orbit Insertion (MOI)**: upon arrival the spacecraft need to be captured by the planet and to do so the engines shall deliver a big amount of propellant (approximately 1000 $\frac{\text{m}}{\text{s}}$). After this kick, the spacecraft enters a highly elliptical orbit: pericentre altitude of 427 km near the South Pole, high inclination (93.5°), a period of 35 h [8](that stems from an eccentricity around 0.85 and an apocenter altitude around 48 000 km);
- **Aerobraking**: the PSO shall be nearly circular, so the orbit needs to be circularized by reducing its eccentricity lowering the apocentre altitude. Since such a maneuver requires large amount of propellant consumption, this Δv shall be gained using the atmospheric drag on the spacecraft. This phase is the longest one and can be subdivided in:
  - **Walk-in**: during this phase the pericenter altitude is gradually lowered up to 105.3 km and this altitude is a good compromise between the atmospheric drag slowdown and the freestream heating rate limits of the spacecraft;
  - **Braking**: at this phase, the apoapsis of the orbit capture will be gradually lowered through atmospheric dips. This sub-phase takes up about 4 and half months and shall continue until the orbit lifetime (that is time it takes the apoapsis altitude of the orbit to decay to an

altitude of 300 km) of the orbiter reaches two days. Performing some calculations based on energetic balance, this braking phase saves 1197 $\frac{m}{s}$ of Δv. Over the braking phase time span of the apoapsis altitude shall be lowered at 450 km; [5]

- **Walk-out**: once reached the threshold of two days orbit lifetime, the periapsis altitude will be lifted at 220 km, and the spacecraft shall remain in this parking orbit for 3 days before the Transition Phase to the PSO;

- **Transition**: during this phase, few orbit adjustments shall be performed to target the PSO:
  - **OA-1**: this first kick shall be performed at apocenter over the North Pole to raise the periapsis altitude to 315 km to match that of the PSO;
  - **IA-1**: A follow-up inclination change maneuver shall be executed on the nodal line to get at PSO's inclination. From the performed calculations it's clear that the inclination change of 0.8° with respect to orbit after MOI (since the objective is 92.7° inclination) has a larger cost than the one listed in the literature, so it's possible that the inclination change has a different angle;
  - **OA-2**: A final consisting of two burns, one at the pericenter over the South Pole to circularize the orbit, and the other over at the North Pole to attain the targeted PSO;

1.2 Station keeping

The cost per year of the station keeping has been performed referring to a linear quadratic model predictive control (LQ-MPC) for Areostationary Mars Orbit [1], which is not the case for this mission but it is possible to retrieve a conservative Δv estimation. From this, considering an orbit correction every 4 weeks [3] that corresponds to ∼358 orbits, it is possible to compute an estimation of the Δv that has been considered of 30 $\frac{m}{s}$ per year.

1.3 Cost breakdown

PHASE	LITERATURE Δv	COMPUTED + MARGIN Δv
Cruise	10 $\frac{m}{s}$ [8]	20 $\frac{m}{s}$
MOI	1015 $\frac{m}{s}$ [2]	1012 $\frac{m}{s}$
Walk-in	14.5 $\frac{m}{s}$ [9]	25 $\frac{m}{s}$
Walk-out	25 $\frac{m}{s}$ [5]	38 $\frac{m}{s}$
OA-1	17 $\frac{m}{s}$ [9]	32 $\frac{m}{s}$
IA-1	18 $\frac{m}{s}$ [9]	48 $\frac{m}{s}$
OA-2	52 $\frac{m}{s}$ [9]	55 $\frac{m}{s}$
Station keeping for 4 years	-	240 $\frac{m}{s}$

Table 1: Maneuvers cost

	FROM LITERATURE	COMPUTED	ONBOARD
TOTAL Δv	1151.5 $\frac{m}{s}$	1470 $\frac{m}{s}$	1545 $\frac{m}{s}$ [2]

2 Propulsion system

The Mars Reconnaissance Orbiter (MRO) employed a monopropellant hydrazine (N_2H_4) propulsion system, divided into primary propulsion for large maneuvers and secondary propulsion for attitude control and minor adjustments.

Engine Type & Data	**Notes**
Primary Propulsion System: MR-107N: 6 Units, 170 N of thrust each [6]	They are installed in a symmetrical cluster and are fired simultaneously. The main reason for choosing to use six relatively small engines rather than a single larger one was to grant redundancy: if one engine fails, MRO could still rely on the other engines, maintaining a coarse thrust alignment.
Secondary Propulsion System: MR-106E: 6 Units, 22 N of thrust per unit [6]	The secondary propulsion system was a backup and a complement to the primary propulsion system, responsible for attitude control maneuvers and momentum management. This system was composed of two distinct thruster types, each optimized to carry out specific tasks. The MR-106E were used for mid-range Δv.
Secondary Propulsion System: MR-103D: 8 Units, 0.9 N per unit [6]	For steady state, I_{sp} was $\sim$ 216 s [4] for continuous firing (e.g., during RCS maneuvers). The pulse-mode I_{sp} varied based on duty cycle: it was initially modeled at 120 s, later adjusted to 147 s for better accuracy.

Table 2: Primary & Secondary Propulsion System [6]

2.1 TCS Phases and functionalities

Engine Type	**Phases**	**Functionalities**	**Notes**
MR-107N	TCM1 and MOI	Navigation to ensure best possible arrival at Martian orbit.	At first, TCM1 was to be executed by MR-106E thrusters, but it was decided to perform it with MR-107N as risk reduction management.
MR-106E	All TCMs excluding the first one and thrust vectoring control during MOI and aerobraking.	Navigation, thrust vectoring, and attitude control during MOI and aerobraking.	Although it was not an intended purpose of these engines at first, during ESP (2015) they performed an orbital maneuver to put the spacecraft in the right place to support arrival of InSight Mars lander mission.
MR-103D	MOI, Aerobraking, PSP, and ESP phases.	Help maintain the aerobraking drag attitude and attitude control during PSP and ESP phases.	Was used together with MR-106E thrusters for attitude control during aerobraking.

Table 3: TCS engines phases & functionalities [8] [7]

2.2 Tank and Feeding System

The 20 thrusters consume hydrazine, which is stored as a liquid and has a wide range of duty cycles. The engines are fed from a single propellant tank mounted near the center of the main bus, and it is sized to accommodate 1220 kg of hydrazine. [2] Furthermore, a separate pressurant gas tank is used to force propellant to the motors by feeding helium gas at high pressure through a regulator into the propellant tank, so the fuel is maintained under pressure. To maintain reliable thruster operation, a minimum of 0.69 MPa tank pressure is necessary. [8]

The feeding system operates in a *blow-down mode* for all mission phases with the exception of MOI where it is *pressure regulated* to provide higher thrust and lower finite burn losses. In the MRO, there is a separate tank to store the helium gas, but the concept of the blow-down strategy is the same as that of the more traditional configuration: a shared tank for both pressurant gas and propellant. This last consideration has been made by observing the figure 2. Lines, valves, and regulators consent the flow of the pressurized hydrazine through metal tubes to each thruster, and each one has a valve so it is independent from the others.

Figure 2: MRO tanks configuration: pressurant tank (white) and propellant tank (red)

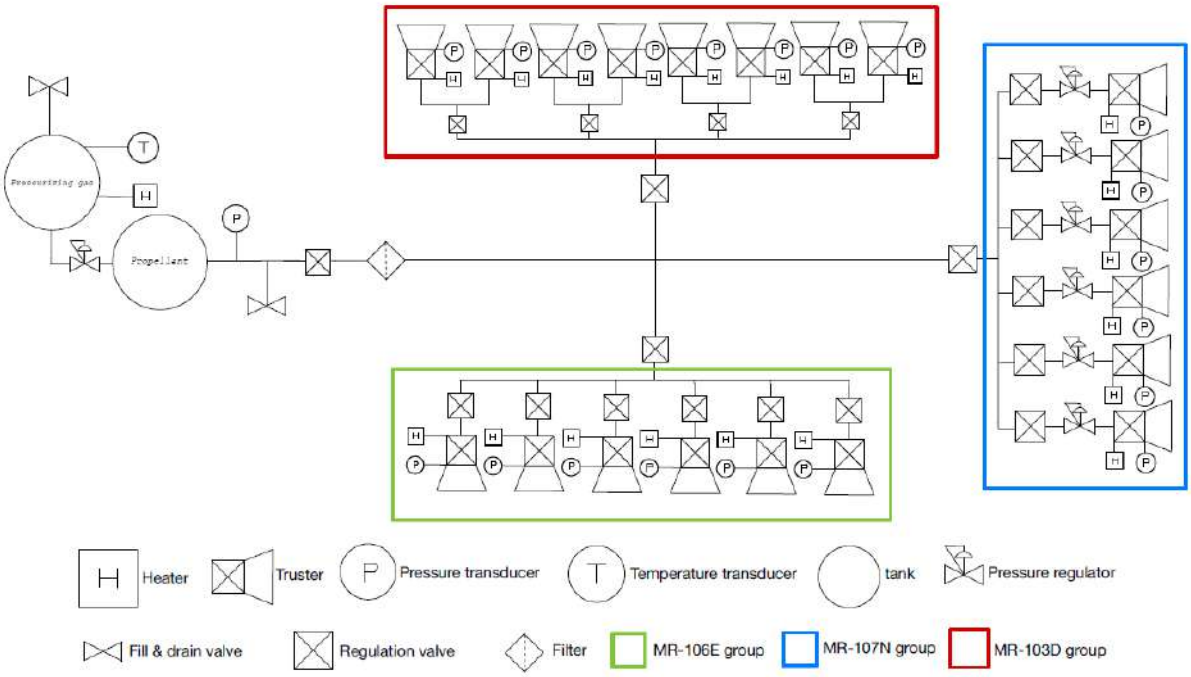

Figure 3: Propulsion System Schematics (made by the team)

2.3 Thrusters configuration

To provide translational control of the spacecraft, the six MR-107N thrusters and six MR-106E thrusters were exploited while the smallest eight MR-103D thrusters oriented the spacecraft, working as an alternative attitude-control system. The figure 4 shows the locations of the thrusters. A1 through A8 are the Attitude Control System thrusters, T1 through T6 are the TCM thrusters, and M1 through M6 are the main engine thrusters. Arranged in couples, the ACS thrusters are fired in pairs, so that ideally the resulting net Δv is zero. The main engine thrusters are located along the positive direction of the Y-axis (roll) as shown in the figure 4 and they are inserted close to the propellant tank, arranged in a circle. This configuration was chosen to avoid the introduction of rotational torque resulting from an asymmetric firing. In this way, the resultant thrust vector passes directly through the center of mass.

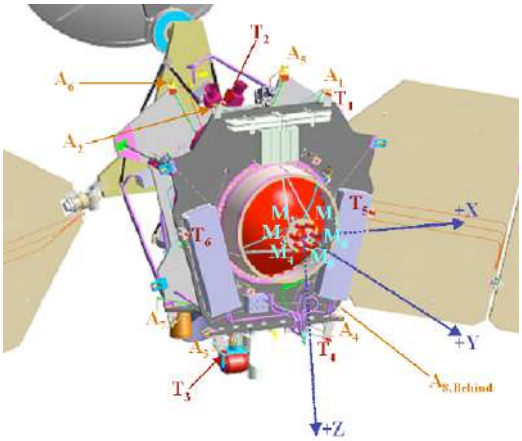

Figure 4: MRO thrusters configuration [8]

2.4 Reverse Sizing

In order to compute the reverse sizing of the volume of the tanks and of the mass of the entire Propulsion System, we considered the following data, taken from literature, that is shown in Table 4:

Δv [2]	M_{dry} [5]	$M_{dry_{real}}$	I_{s1} [4]	I_{s2} [4]	I_{s3} [4]	ρ_{prop}	$P_{c_{max}}$ [4]	$P_{c_{min}}$ [4]
1545 m/s	981 kg	1177 kg	230 s	232 s	216 s	1010 kg/m^3	2.34 MPa	0.42 MPa

Table 4: Data considered for reverse sizing

On the dry mass was applied a margin of 20%, while the data of the Δv was already taken with the margin from literature. The Δv budget can be divided into 3 parts, each related to a group of thrusters and a certain operation, MOI for the main engines (MR-107N) and attitude control for the others:

MR-107N [2]	MR-106E [5]	MR-103D [5]
1015 m/s	380 m/s	150 m/s

Table 5: Δv division

2.4.1 Propellant tank volume

After dividing the Δv budget, we can compute the mass of propellant needed for each group of thrusters using the Tsiolkowsky equation to evaluate the mass ratio (MR):

$$MR = \frac{M_{wet}}{M_{dry_{real}}} = e^{\frac{\Delta v}{I_s g_0}} \tag{1}$$

To the propellant mass was added a total margin of 5.5% in order to account for ullages, residuals and loading uncertainties. The volume of the propellant was then computed and a 10% margin was then added. The volumes and masses of propellant relative to the 3 groups of thrusters are shown in Table 6

M_{prop_1}	M_{prop_2}	M_{prop_3}	$M_{prop_{tot}}$	V_{prop_1}	V_{prop_2}	V_{prop_3}	$V_{prop_{tot}}$
705.52 kg	225.68 kg	91.10 kg	1022.3 kg	0.7684 m^3	0.2458 m^3	0.0992 m^3	1.1134 m^3

Table 6: Masses and volumes of propellant

Since the propellant and pressurant tanks are separate, the volume of the propellant tank corresponds to the one of the propellant.

2.4.2 Pressurant tank volume

In order to compute the volume of the pressurant tank, we need to remember that MRO uses both a pressure-regulated system, used primarily for the main thrusters and for the MOI, and a blow-down system for the pressurization. Starting with the pressure regulated system for the main thruster, the formula to calculate the mass of helium is:

$$M_{gas_{PR}} = \frac{P_{tank} V_{prop}}{R_{gas} T_{tank}} \frac{\gamma}{1 - \frac{P_{gas,f}}{P_{gas,i}}} \tag{2}$$

Where $P_{tank} = P_{c_{min}} + \Delta P_{inj} + \Delta P_{feed} = P_{gas,f}$, $P_{gas,i} = 10 P_{tank}$, $\Delta P_{feed} = 35.5$ kPa, $\Delta P_{inj} = 30\% P_{c_{min}}$, $\gamma = 1.67$ and $T_{tank} = 293$ K. A margin of 20% was applied to the mass of the gas. For the blow-down system, in order to compute the gas mass we must first calculate the blow-down ratio:

$$B = \frac{P_{gas,i}}{P_{gas,f}} \tag{3}$$

$$V_{gas_{BD}} = \frac{V_{prop}}{B - 1} \tag{4}$$

In order to compute the mass of the gas, the ideal gas law was used. Additionally, a margin of 20% was added to the pressurant mass. The results of these computations are shown in Table 7

$M_{gas_{PR}}$	$V_{gas_{PR}}$	B	$M_{gas_{BD}}$	$V_{gas_{BD}}$	$M_{gas_{tot}}$	$V_{gas_{tot}}$
2.69 kg	0.1711 m^3	5.6723	0.79 kg	0.0793 m^3	3.47 kg	0.2504 m^3

Table 7: Masses and volumes of pressurant

2.4.3 Tank sizing and mass budget

The last step to compute the mass budget is computing the masses of the tanks. Since no feedbacks were found in the literature, we assumed the tanks to be cylindrical with hemispherical caps and to be made of titanium (Ti6A14V). With these assumptions in mind, we were able to calculate the mass of both tanks:

ρ_{tanks}	σ_{Ti}	$M_{tank_{prop}}$	$M_{tank_{gas}}$	M_{tanks}
2780 kg/m^3	950 MPa	28.76 kg	7.76 kg	36.52 kg

Table 8: Tank masses and Titanium characteristics

The total mass budget of the Propulsion System is obtained by:

$$M_{Tot} = M_{gas} + M_{tanks} + \sum_i n_{thruster_i} M_{thruster_i} \tag{5}$$

The final data are reported in Table 9; a margin of 10% was added to the total mass of the propulsion system.

$n_{MR-107N}$	$M_{MR-107N}$ [4]	$n_{MR-106E}$	$M_{MR-106E}$ [4]	$n_{MR-103D}$	$M_{MR-103D}$ [4]	M_{PS}
6	1.01 kg	6	0.635 kg	8	0.33 kg	57.75 kg

Table 9: Mass of Propulsion System

2.4.4 Power Budget

The power budget can be determined by studying the power consumption of the thrusters valves and feeding system, multiply them by the number of each thruster and adding them together:

$W_{MR-107N}$[4]	$W_{MR-106E}$ [4]	$W_{MR-103D}$ [4]	W_{Tot}
34.8 W	42, 79 W	13, 72 W	575.3 W

Table 10: Power of Propulsion System

2.4.5 Conclusions

No data has been found regarding the mass of the pressurant stored inside of the MRO nor of its tank volume. However, the total mass of propellant on board at launch was 1149 kg, while the tank was designed to hold up to 1220 kg of propellant [2]; the discrepancy with the mass obtained through reverse sizing is due to multiple reasons: simplifying assumptions in the specific impulses of the thrusters and not accounting for the reserve propellant added last minute thanks to a dry mass lighter than anticipated.

References

[1] Nathan A Gall, Robert D Halverson, and Ryan J Caverly. "Station Keeping of Areostationary Mars Orbit Satellites using Linear Time-Varying Model Predictive Control". In: *AAS/AIAA Astrodynamics Specialist Conference*. 2024.

[2] James E. Graf et al. "The Mars Reconnaissance Orbiter Mission". In: *Acta Astronautica* 57.2 (2005). Infinite Possibilities Global Realities, Selected Proceedings of the 55th International Astronautical Federation Congress, Vancouver, Canada, 4-8 October 2004, pp. 566–578. ISSN: 0094-5765. DOI: https://doi.org/10.1016/j.actaastro.2005.03.043. URL: https://www.sciencedirect.com/science/article/pii/S0094576505000780.

[3] Dolan Highsmith et al. "Mars Reconnaissance Orbiter navigation during the primary science phase". In: *AIAA/AAS Astrodynamics Specialist Conference and Exhibit*. 2008, p. 6422.

[4] Aerojet Rocketdyne Holdings Inc. In: URL: https://satsearch.co/products/aerojet-rocketdyne-mr-106e-28vdc.

[5] Martin D Johnston et al. "The Mars Reconnaissance Orbiter mission: From launch to the primary science orbit". In: *2007 IEEE Aerospace Conference*. IEEE. 2007, pp. 1–19.

[6] Robert E Lock et al. "The Mars reconnaissance orbiter mission plan". In: (2004).

[7] NASA. URL: https://www.jpl.nasa.gov/news/nasa-mars-orbiter-preparing-for-mars-landers-2016-arrival/.

[8] Tung-Han You et al. "Mars Reconnaissance Orbiter interplanetary cruise navigation". In: *Proceedings of the 20th International Symposium on Space Flight Dynamics*. 2007.

[9] Tung-Han You et al. "Navigating Mars reconnaissance orbiter: Launch through primary science orbit". In: *AIAA SPACE 2007 Conference & Exposition*. 2007, p. 6093.

MRO Reverse Engineering Study

Assignment #3

Team 21

P. Code	Surname	Name
10724393	Chini	Filippo
10721870	Mazzitti	Riccardo
10682521	De Gennaro	Antonio
10764250	Bianco	Emanuele
10668777	Matteotti	Luca
10810285	Basci	Matteo Maria
11076681	Kazenas	Mantas

Space System Engineering and Operations

Prof: M. Lavagna

L. Bianchi, M. Bussolino

M.Sc Space Engineering
A.Y. 2024-2025

Change log	
Issue	*Comments*
1	First release

Contents

1 Design and Architecture **1**
1.1 Ground infrastructure 1
1.2 TMTC subsystem architecture 1
1.2.1 Antennas onboard 1
1.2.2 Transponders 2
1.2.3 TWTA panel 2
1.2.4 Electra module 3

2 Phases, operations and data volumes **4**

3 Reverse sizing of TMTC subsystem **5**
3.1 X-band Downlink 5
3.2 X-band Uplink 6

List of Acronyms	
Acronym	*Full Name*
MEP	Mars Exploration Program
TMTC	Tracking Telemetry and TeleCommunications subsystem
MOI	Mars Orbit Insertion
DSN	Deep Space Network
BWG	Beam Wave-Guide
HEF	High EFficiency
HGA	High Gain Antenna
CEP	Circular Error Probability
RCP	Right Circularly Polarized
LGA	Low Gain Antenna
SDST	Small Deep-Space Transponders
DOR	Differential One-way Ranging
TWTA	Traveling Wave Tube Amplifier
LVDS	Low-Voltage Differential Signaling
FPGA	Field Programmable Gate Array
QPSK	Quadrature Phase-Shift Keying
DOR	Differential One-way Ranging
LPF	Low Pass Filter
HVPS	High-Voltage Power Supply
UHF	Ultra High Frequency
BPSK	Binary Phase-Shift Keying

1 Design and Architecture

One of the main mission goals for MRO was to provide support for Mars Exploration Program (MEP) and landed missions with communication relay to enhance the data return and communications capabilities. Thus, it was clear from the start of design phases that a lot of resources and development time shall be spent on the architecture and solutions for Tracking Telemetry and Telecommunications subsystem (TMTC).[3]

1.1 Ground infrastructure

The Mars Reconnaissance Orbiter relies on Deep Space Network stations with antennas located in Goldstone California, Madrid Spain and Canberra Australia.[2] The orbiter spends around one third of its time behind Mars from the viewpoint of Earth and during this period the orbiter is hidden and cannot communicate with Deep Space Network antennas located on Earth. [3]
During cruise and orbit operations, MRO was allocated the 70 m wide antenna subnet (which was also used for the o Mars orbit insertion, MOI), the 34 m beam-waveguide (BWG) antenna subnet and the 34 m High Efficiency (HEF) antenna subnet. [3]
For the vast majority of its nominal telemetry and commanding operations, MRO relies on 34 m BWG antennas. The operating ground network has largely remained unchanged over time and still, it mostly operates from the same locations as at the beginning of the mission, however, the operating time has been modified to prioritize newer missions requiring same or similar infrastructure. [3]
It is also possible for MRO mission to be allocated the 34 m HEF stations (at the same operating locations) for usage that do not require Ka-band downlink capabilities.[3]

1.2 TMTC subsystem architecture

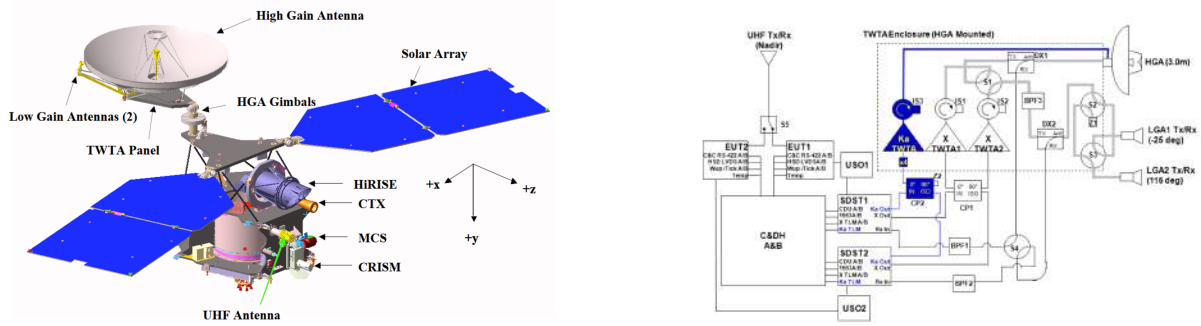

(a) (b)

Figure 1: (a) MRO instrument placement[3] (b) MRO TMTC subsystem schematic[3]

1.2.1 Antennas onboard

- **High-gain antenna:** MRO main antenna has a diameter of 3 meter. The HGA is mounted on a two-axis gimbal, allowing it to steer toward Earth without requiring the whole spacecraft to reorient. The requirement for HGA pointing accuracy is 2.08 mrad with a 99.7% circular error probability (CEP). The HGA consists of three main components: the feed, an ellipsoidal subreflector, and a 3 meter offset parabolic main reflector. The HGA subreflector is 0.45 meter in diameter and is located near the focal point of the main reflector. The X-band feed is a corrugated horn design, while the Ka-band feed is a disc-on-rod design. There is no uplink

reception at Ka-band but only downlink transmission. The feeds contain polarizers at X-band and at Ka-band in order to generate right-circularly-polarized (RCP) microwaves.

- **Low-gain antennas:** MRO has two low-gain antennas that have lower data-rate capabilities compared to high-gain antenna, because they were designed to be used for special events during mission, such as launch, MOI and safe mode. These antennas are designed as a horn and are placed on the opposite side of one another in order to emit radio beams much wider than the high-gain antenna which ensures uplink and downlink no matter the orientation of the satellite.

1.2.2 Transponders

MRO has 2 Small Deep-Space Transponders (SDST), which are redundant and provide the same function, that were already used in other missions such as Deep Space 1, Mars Odyssey and MER [3]. The SDST has multiple scopes which include: track the uplink carrier and demodulate commands from it; generate the downlink carrier; perform convolutional coding; produce different subcarrier frequencies and modulate telemetry on the subcarrier; generate Differential One-way Ranging (DOR) tones. [3]
With respect to previous implementations, the MRO's SDST have a different design that includes: [3]

- A x4 (times-four) multiplier that is used to generate the 32.2-GHz Ka-band signal from the 840f1 (f1 is the fundamental frequency from which the uplink and downlink frequencies are derived) frequency output (8052 MHz). It's placed on the TWTA panel, this is done to minimize coaxial cable loss at Ka-band.
- Low-Voltage Differential Signaling (LVDS) receivers, that are in the digital processing module (DPM), to support high-rate transmission over the compact Peripheral Component Interconnect (cPCI) bus.
- A field programmable gate array (FPGA) with 72 thousand gates has been added to the MRO SDST to support quadrature phase-shift keying (QPSK). The FPGA also performs (7,1/2) convolutional coding for QPSK.
- Wideband DOR (8f1 DOR) capability has been added at Ka-band.
- An internal five-pole, 5.8MHz low-pass filter (LPF) is also present in the SDST. It filters the input voltage to the phase modulator. By default, the MRO SDST operates in filtering mode in order to reduce high-frequency component in the telemetry downlink. This minimizes the risk of interference with other missions and the unfiltered mode may only be used when there is no risk for spectral interference.

1.2.3 TWTA panel

At the back of the high-gain antenna there is an enclosure for the Traveling-Wave Tube Amplifiers (TWTAs) and associated microwave components (figure 2).
There are three amplifiers on board, two at X-band (redundant), with a frequency output power of 100 W, and one at Ka-band, with a frequency output power of 35 W [3]. The TWTAs were chosen for their history of high power efficiency and performances at high frequencies, in particular in deep-space communications from the past missions, and their ability to operate at both X-band and Ka-band frequencies, which provides redundancy and flexibility for MRO mission. The amplifiers also include the High Voltage Power Supply (HVPS), the traveling-wave tube (TWT) and the diplexers.[3]
The latter allow to route X-band transmissions and receiving frequency signals that are present simultaneously at the antenna. They have three ports: the antenna port, the receive port and the transmit

port. The transmission and receiving ports must be isolated in order to avoid self-interference within the subsystem.

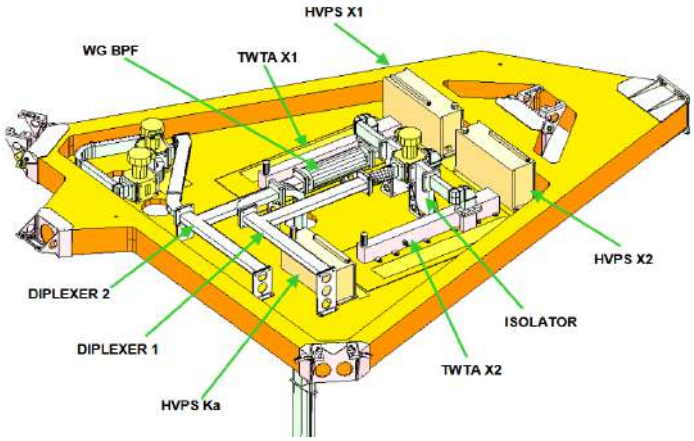

Figure 2: TWTA panel layout [3]

TWTA provides three kinds of protection for the spacecraft power supply and itself: [3]

- **Helix overcurrent trip:** In the event of helix current exceeding 5 mA, the power converter goes into automatic restart mode within 2 ms, which involves removal and reapplication of the high voltage to the TWT.
- **Power Converter Overcurrent Trip:** If the input current exceeds a maximum value, the switching transistor is protected by cycle peak current limitation and after 2 ms, the converter goes into automatic restart mode.
- **Bus Undervoltage Trip:** If the bus voltage at the converter input drops below 20.5 V, the high voltage switches off and an undervoltage trip status flag is set. When the bus voltage rises above 20.5 V again, the TWTA startup sequence is initiated and starts the preheating process, which lasts about 210 s. The nominal bus voltage is 28 V.

1.2.4 Electra module

The Electra communications package is an UHF radio, that provides possibilities for MRO to support and relay transmissions from Mars landers and rovers. It allows the MRO to become a network node in the mars network constellation that provides efficient relay of high-rate science and engineering data [1]. The use of Electra increases the amount of data returned from Mars by two to three orders of magnitude.

2 Phases, operations and data volumes

The MRO mission was designed to return a huge amount of data from Mars; over its 2-year primary science mission, MRO transmitted more than 34 terabits of data thanks to the high-gain antenna and the 100-watt X-band traveling-wave tube amplifier (TWTA), which enabled data rates up to 6 Mbps during favorable Earth-Mars distances. [3].

MRO normally scheduled two 34-meter Deep Space Network passes daily during the primary science phase, providing an average of 16 hours of coverage per day. Twice a week, 70-meter antennas were added for additional support. Depending on the distance between Earth and Mars, this allocation enabled MRO to send data for 10–11 hours every day at an average rate of 0.5–4 Mbps.

Table 1 showcases what antennas were used during different mission phases and events, their Uplink & Downlink rates and what purpose they served during those mission phases.

Phase	**Used Antennas**	**Uplink & Downlink rates**	**Usage**
Launch & Cruise	Low-gain antennas	Low rate Uplink/Downlink (up to a few kbs)	Communications start, tracking, health monitoring
MOI	Low-gain antennas	Moderate-rate (few kbps to $\sim$ 32 kbps)	Tracking, telemetry, system checks and command
PSP	High-rate antenna	Downlink: up to 6 Mbps Uplink: $\sim$ 2 kbps	Main science data return to Earth, command uplink
ESP	High-gain antenna	Downlink: up to 6 Mbps Uplink: $\sim$ 2 kbps	Additional science data return to Earth, command uplink
Extended relay mission	High-gain antenna	Continued high-rate downlink	Continued support for surface missions on Mars
Special operations & events			
Relay Operations	UHF antenna	128–256 kbps (to/from rovers/landers)	Relay communications for landers/rovers
Emergency mode	Low-gain antennas	Low rate Uplink/Downlink (up to a few kbs)	System checks and command

Table 1: MRO Telecommunications to phases and its usage [2], [3]

3 Reverse sizing of TMTC subsystem

For the sizing of the telecom subsystem it was taken into consideration the fact that MRO communicates with Earth mainly with its HGA using a X-band frequency of $f_{X-band} = 8.41\,\text{GHz}$ for both downlink and uplink communications. MRO uses a convolutional encoding ($k = 7$, $r = \frac{1}{2}$) [3] that corresponds to $\alpha_{enc} = 2$, while for modulation it uses both BPSK ($\alpha = 1$) and QPSK ($\alpha = 2$), which results in a total $\alpha_{mod} = 2$ [3]. The data rate value can range from 500 kbps up to 4 Mbps [3] but in this report the worst case scenario (when the spacecraft is at the maximum distance from Earth of 400 million kilometer) is taken into consideration, so the minimum value is taken. Regarding the power supply, since the amplifiers are TWTA, only $\mu_{ampl} = 60\%$ of the power is transformed into RF power.
An important assumption that was made affects the pointing losses; the equation for computing them is:

$$L_{point} = -12\left(\frac{e}{\theta_{rx}}\right)^2 \tag{1}$$

where e is the misalignment angle between the TX and RX antennas and θ_{rx} is the RX antenna beam-width. For a misalignment angle of 2 mrad, by using this formula, the result ($\sim 30\,\text{dB}$) differed greatly from the one from literature ($0.2\,\text{dB}$ [3]), as seen in figure 3:

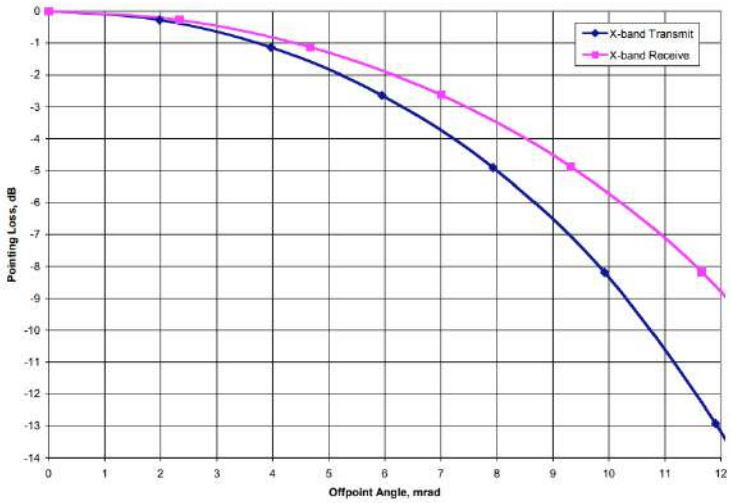

Figure 3: Pointing losses [3]

This significant difference between real and theoretical values is due to the fact that the equation is imprecise and leads to incorrect results.

3.1 X-band Downlink

For the downlink sizing, in order to respect the conditions $SNR \geq SNR_{min}+3$ dB and $\frac{E_b}{N_0} \geq \frac{E_b}{N_0\,min}+3$ dB, the available transmitter power should be $P_{tx} = 140\,\text{W}$. This value diverges from the one from the literature ($P = 100\,\text{W}$ [3]) and this is due to the coarse approximations of different values such as the roll of factor (0.5) and the signal losses. The results of the sizing are shown in table 2.
A pivotal parameter, also for OBDH, is the average data volume per contact, which, in the reverse sizing, is calculated over the timespan of the entire designed mission (2 synodic periods). The energy per bit level shall be fixed at $8.37dB$ and the net data rate that varies with the distance from Earth is capped at $4Mbps$ when the spacecraft is close enough to Earth, with the largest allowable contact

window for downlink of 10h, because MRO shall not interfere with other missions' communications on DSN [3], and the fetched daily average downlink data is $59.97 Gbits$, which also encompasses the unreliable data in Solar Conjunctions:

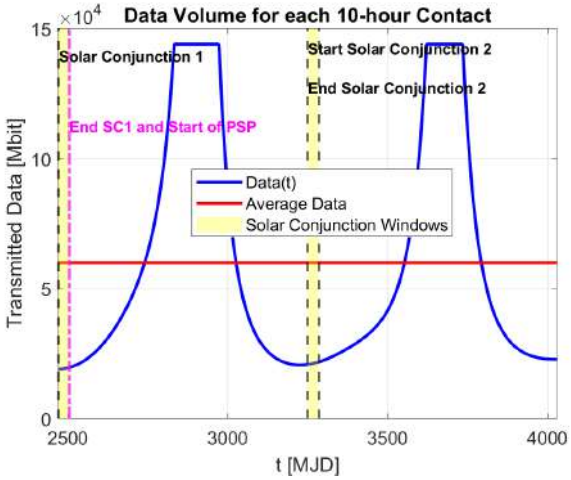

Figure 4: Average vs Time/Distance-dependant Transmitted data volume during each 10-hour contact

3.2 X-band Uplink

For the uplink sizing, of the available output power $P = 20kw$ from the $34m$ BWG [3], only $2kw$ yield $E_b/N_0 = 10.46dB > E_b/N_{0min} = 7.5dB$ and a $SNR = 8.70dB > SNR_{min} = 5.74dB$. The reason for the choice of the ground antenna transmitted power is a reasonable compromise between the save in power use and the counteraction on the effect from the receiver system noise temperature, which adds up to the already existing free space losses.

Parameter	Value
Transmitted power (P_{tx})	21.5 dB
TX antenna gain (G_{tx})	45.8 dB
RX antenna gain (G_{rx})	66.9 dB
Cable losses (L_{cable})	−1 dB
Pointing losses (L_{point})	−0.2 dB
Atmospheric losses (L_{atm})	−0.05 dB
Free space losses (L_{space})	−283 dB
Bandwidth (B)	750 kHz
Net datarate (R_{net})	500 kbps
Gross datarate (R_{gross})	500 kbps
RX system noise temperature (T)	21 K
Minimum E_b/N_0 (+ 3 dB margin)	8 dB
Minimum SNR (+ 3 dB margin)	6.24 dB
E_b/N_0	8.37 dB
SNR	6.61 dB

(a) MRO link budget downlink

Parameter	Value
Transmitted power (P_{tx})	23.0 dB
TX antenna gain (G_{tx})	66.9 dB
RX antenna gain (G_{rx})	45.8 dB
Cable losses (L_{cable})	−1 dB
Pointing losses (L_{point})	−0.2 dB
Atmospheric losses (L_{atm})	−0.05 dB
Free space losses (L_{space})	−283 dB
Bandwidth (B)	48 kHz
Net datarate (R_{net})	32 kbps
Gross datarate (R_{gross})	32 kbps
RX system noise temperature (T)	290 K
Minimum E_b/N_0 (+ 3 dB margin)	7.5 dB
Minimum SNR (+ 3 dB margin)	5.74 dB
E_b/N_0	10.46 dB
SNR	8.70 dB

(b) MRO link budget uplink

Table 2: Sizing results for downlink and uplink

References

[1] Charles D. Edwards. "The Electra Proximity Link Payload for Mars Relay Telecommunications and Navigation". In: *54th International Astronautical Congress of the International Astronautical Federation, the International Academy of Astronautics, and the International Institute of Space Law*. DOI: 10.2514/6.IAC-03-Q.3.a.06. eprint: https://arc.aiaa.org/doi/pdf/10.2514/6.IAC-03-Q.3.a.06. URL: https://arc.aiaa.org/doi/abs/10.2514/6.IAC-03-Q.3.a.06.

[2] James E Graf et al. "The Mars reconnaissance orbiter mission". In: *Acta Astronautica* 57.2-8 (2005), pp. 566–578.

[3] Jim Taylor, Dennis K Lee, and Shervin Shambayati. "Mars reconnaissance orbiter". In: *Deep Space Communications* (2016), pp. 193–250.

MRO Reverse Engineering Study

Assignment #4

Team 21

P. Code	Surname	Name
10724393	Chini	Filippo
10721870	Mazzitti	Riccardo
10682521	De Gennaro	Antonio
10764250	Bianco	Emanuele
10668777	Matteotti	Luca
10810285	Basci	Matteo Maria
11076681	Kazenas	Mantas

Space System Engineering and Operations

Prof: M. Lavagna

L. Bianchi, M. Bussolino

M.Sc Space Engineering
A.Y. 2024-2025

Change log	
Paragraph	*Comments*
2.2.1	pp.3-4 Reaction wheels text corrected and simplified, data added: mean deviation angle
2.2.2	pp.5 Propellant mass and number of desaturations changed, formula of propellant mass corrected
2.3	pp.6 Accuracy of Observation Mode and Safe Mode changed

Contents

1 Mission AOCS architecture **1**
1.1 Attitude Sensors . . . 1
1.2 Actuators . . . 1
1.3 Control Modes . . . 1

2 ADCS Sizing **3**
2.1 Disturbances effects . . . 3
2.1.1 Gravity Gradient . . . 3
2.1.2 Air drag and SRP . . . 3
2.2 Actuators sizing . . . 3
2.2.1 Reaction wheels . . . 3
2.2.2 Thrusters . . . 4
2.3 Pointing budget . . . 6
2.4 Mass and Power budgets . . . 6

List of Acronyms	
Acronym	*Full Name*
AOCS	Attitude and Orbit Control System
IMU	Inertial Measurement Unit
RCS	Reaction Control System
SAM	Sun Acquisition Mode
OTM	Orbit Trim Maneuver
HGA	High Gain Antenna
SRP	Solar Radiation Pressure
GGT	Gravity Gradient Torque
RW	Reaction Wheels
AKE	Absolute Knowledge Error
APE	Absolute Pointing Error

1 Mission AOCS architecture

The MRO Attitude and Orbit Control System (AOCS) integrates sensors, actuators, and control logic to achieve precise pointing and orbital stability. The AOCS is divided into 3 general parts: attitude sensors, actuators and the different control modes.

1.1 Attitude Sensors

The AOCS relies on multiple attitude sensors to determine the orientation of the spacecraft relative to the Sun, stars, and Mars [11]; the key sensors used are the following:

- **Star trackers:** There are two onboard star trackers that provide full 3-axis attitude determination via star pattern recognition allowing MRO to know where Sun, Earth and Mars are, and how to point anywhere in space (crucial for maneuvering). Moreover, one tracker serves as a backup.[5] Since 2018, MRO has transitioned to an "all-stellar" mode, relying more on star trackers to reduce gyro usage. In the design mission lifetime, they were used only for safe mode. [16]
- **Sun Presence Sensors:** MRO has sixteen sun sensors (eight as backup) and they are mounted around the spacecraft to detect the presence of the Sun by returning a simple "sun" / "no sun" signal. By processing these signals, the spacecraft can determine the sun's location, which is crucial for power generation. As they are not precise enough for tasks such as locating Earth for communication or finding precise locations on Mars, it was chosen to only use them on initial activation (post-launch) and for emergencies.[5]
- **Inertial Measurement Units (IMU):** Two Inertial Measurement Units (IMUs) are onboard MRO, with one serving as a backup. Each IMU combines three accelerometers and three ring laser gyroscopes (accelerometers measure change in speed, while gyroscopes measure rotation rates). IMUs can also estimate orientation during periods when start trackers are ineffective, for example, when the spacecraft is turning too fast for the star tracker to work properly.[5]

1.2 Actuators

MRO uses a combination of actuators in its AOCS to maintain precise orientation, perform orbital maneuvers, and ensure stability for high-resolution imaging; the key actuators are:

- **Reaction Control System thrusters:** In total there are eight Reaction Control System (RCS) thrusters onboard. These thrusters adjust the spacecraft's rotation. They are arranged in "couples" to prevent rotational maneuvers from providing any lateral velocity (unlike larger thrusters). In case one thruster in a pair should malfunction, the other one can still perform the tasks as long as navigators can measure additional lateral velocity and take it into account in their further calculations. [7]
- **Reaction Wheels:** Reaction wheels are used for precise attitude adjustments when a rapid change in turn rate is not necessary (mostly high-resolution imaging of Mars surface). There are four wheels present; three for each rotational axis and one inserted for redundancy. The wheels are spun using electric motors at various speeds and can reach up to 6000 rpm if necessary. In order to be able to continuously use the reaction wheels, a desaturation maneuver is necessary and is performed by RCS thrusters.[5]

1.3 Control Modes

MRO utilizes several control modes incorporated in its AOCS for all different purposes, the main ones are described below:

- **Safe Hold Mode:**

  Tasks: Stabilize the satellite by detumbling it and determining its attitude, orient the solar panels toward the Sun. Also maintain stability if there is any anomaly with spacecraft, in order for ground control to solve the problem and resume operations.

  Characteristics: Use the most reliable hardware, minimize power consumption, allow for rough pointing accuracy, and ensure fully autonomous operation. [9]

- **Stand-By Mode:**

  Tasks: Point the solar panels towards the Sun and align antennae towards Ground Station.

  Characteristics: Involvement of more complex hardware than Safe Hold Mode, better pointing accuracy than Safe Mode, but potentially not as precise as in Scientific Mode. Typically autonomous with different guidance, navigation, and control (GNC) functions from Safe Mode. [9]

- **Science (Observation) Mode:**

  Tasks: Maintain a precise lock on a Mars surface for scientific mission and smoothly turn the spacecraft accounting for spacecrafts movement.

  Characteristics: Requires very precise accuracy and utilizes most, if not all, available hardware to achieve smooth and precise movement. Functions autonomously, but it is typical to be ground assisted for best performance. [9]

- **Orbital Correction Mode:**

  Tasks: Execute orbital maneuvers to adjust and control the MRO's trajectory.

  Characteristics: Involves the use of propulsion systems, requires management of thrust-induced parasitic torques and is typically ground-assisted to ensure precise orbital corrections.[9]

- **Transfer Mode:**

  Tasks: Control the attitude during transfer to Mars.

  Characteristics: Involves propulsion systems to perform transfers, requires control of thrust-induced parasitic torques. Can operate autonomously, but may be ground-assisted for critical maneuvers. [9]

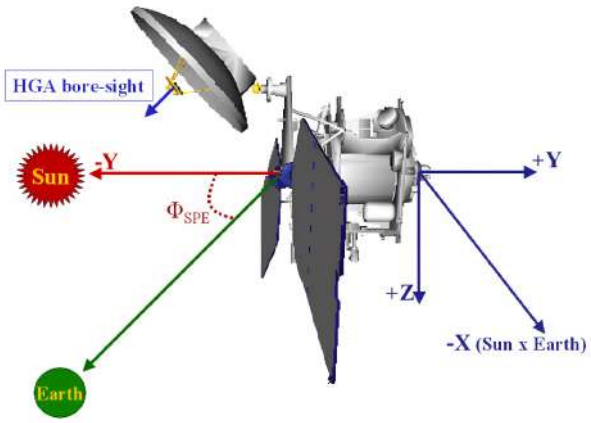

Figure 1: MRO pointing configuration

2 ADCS Sizing

2.1 Disturbances effects

Since the mission orbits around Mars, the magnetic disturbance has a really small contribution, this is due to the weak magnetic field of Mars, and so it has been neglected. The other disturbances have been studied, and the computations are shown in the following paragraphs.

2.1.1 Gravity Gradient

For the Gravity Gradient torque, the general formula is:

$$T_{gg} = \frac{3\mu}{2R^3}(I_{max} - I_{min})sin(2\theta) \tag{1}$$

where μ is the Mars gravitational constant; R is the orbital radius, taken with respect to the pericenter in order to obtain the highest T_{gg} value; θ is the maximum deviation of the z-axis from the local vertical; I_{max} and I_{min} are the maximum and minimum inertia moments of the s/c axes. For the inertia moments the main body of MRO has been assumed a parallelepiped and the solar panels two rectangular plates, the contribution of the HGA has also been taken into account. The data are shown in table 1

μ	42 828.314 $\frac{km^3}{s^2}$	I_{max}	4921.72 kg m^2
R	3645 km	I_{min}	3999.92 kg m^2
θ	30° [16]	T_{gg}	$1.06 \cdot 10^{-3}$ Nm

Table 1: Gravity Gradient data

2.1.2 Air drag and SRP

To compute the air drag and the SRP the following equations have been used:

$$T_{drag} = \frac{1}{2}\rho c_d A v^2 (c_{ap} - c_g) \qquad T_{SRP} = \frac{F_s}{c} A_s (1+q) cos(i)(c_{sp} - c_g) \tag{2}$$

But through computations it was discovered that the contribution of these two disturbances are much smaller than the one from the Gravity Gradient, since $T_{drag} = 2.4265 \cdot 10^{-5}$ Nm and $T_{SRP} = 2.8547 \cdot 10^{-5}$ Nm, and so it was deemed to neglect them.

2.2 Actuators sizing

The actuators' sizing turns on the dominant disturbance, which is then scaled up by a margin of 2 to perform calculations.

2.2.1 Reaction wheels

The RW have two main functionalities: to counteract environmental disturbances and to rotate the spacecraft:

- Accumulation mode: The requirement of 0.5 $\frac{deg}{s}$ shall be set for slew maneuvers so as not to breach the recommended spin rate of RW, which would have inhibit the interaction with the vibration modes of the spacecraft [6], and also to prevent the spacecraft from tumbling out of control. The angular rate limit of the spacecraft has a maximum storable angular momentum of 42.95 Nms, in line with the literature result [15], which would mean a desaturation almost every 3 orbits (2.9949), and a required torque of

0.119 Nm. But from real mission data [16] ,desaturation happens every 48 h, which approximates to 26 orbits. This means that the maximum deviation angle from z-axis of the worst case scenario (30°) is too prohibitive for the entire duration of the mission, so the value of the mean deviation angle during the entire mission has been computed: $\theta = 2.65°$. By taking the rounded number of orbits as a reference to pace actual operations, the storable angular momentum is 43.02 Nms, a value still deemed feasible since the steady-state figure is 44 Nms [12]. The former value of 42.95 Nms is used for the subsequent analysis of the slew mode, because it complies with the maximum angular rate, while the latter is used in the desaturation, because it is closer to the aforementioned steady-state threshold of the angular momentum of RW.

- Slew mode: the RW slew maneuver is divided into an accelerating and a decelerating phase, and the sizing of the RW turns on the worst case scenario of a 180° rotation which can be computed as follows:

$$\dot{\theta}_{slew_{max}} = \frac{1}{2}\frac{T_{slew} t_{slew}}{I_{max}} \tag{3}$$

$$t_{slew} = \sqrt{\frac{4\theta_{slew_{max}} I_{max}}{T}} \tag{4}$$

Despite the sizing, the RWs are not recommended for large slew maneuver, also within the worst case scenario (30° off-Nadir angle around roll axis [16]) due to the large time it takes to perform the slew maneuver that could make the spacecraft lose the target. Indeed, RWs' usage shall be limited to small slew maneuvers to fulfill tight pointing accuracies, that generate very low torques in the spacecraft attitude.

$\dot{\theta}_{max}$	0.5°	T_{slew}	0.119 Nm
t_{slew}	720 s	$h_{max;slew}$	42.95 Nms

Table 2: RW sizing data

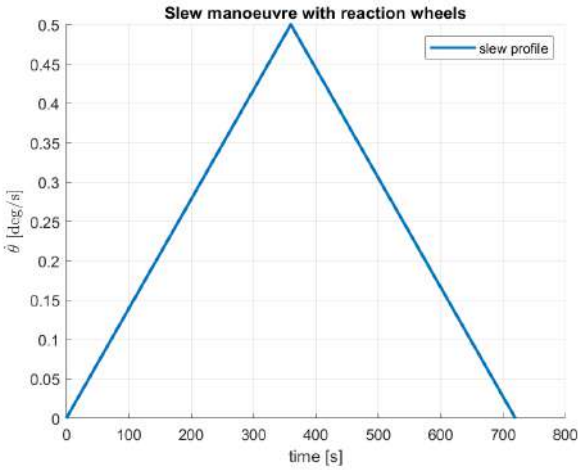

Figure 2: Slew maneuver with RW

2.2.2 Thrusters

The thrusters have 3 main functionalities: counteract the external disturbances, perform slew maneuvers and desaturate reaction wheels. However, the torque from the thrust force is much higher in magnitude

than the GGT, therefore the external disturbances' contribution was neglected for the sizing.

– Slew Mode: the slew maneuvers with thrusters are divided into 3 phases: constant acceleration, coasting and constant braking. The sizing of the thrusters is based on the slew angles summation of each phase $\theta_{slew} = \theta_{acc} + \theta_{coast} + \theta_{brake}$. Moreover, $t_{acc} = t_{brake}$, because the thrusters provide the maximum available force in both phases, and $\theta_{acc} = \theta_{brake}$, because at the coasting phase the spacecraft rotates at the maximum allowable angular speed and because the maneuver is rest-to-rest. By reversing the summation formula, the times for each phase can be computed. The data obtained in this report are shown in table 3:

n_{th}	2	L	1.25 m
F_{th}	0.9 N	$\dot{\theta}_{coast}$	0.5 °/s
t_{acc}	19.09 s	t_{coast}	340.91 s
t_{slew}	379.09 s	-	-

Table 3: Thruster sizing data

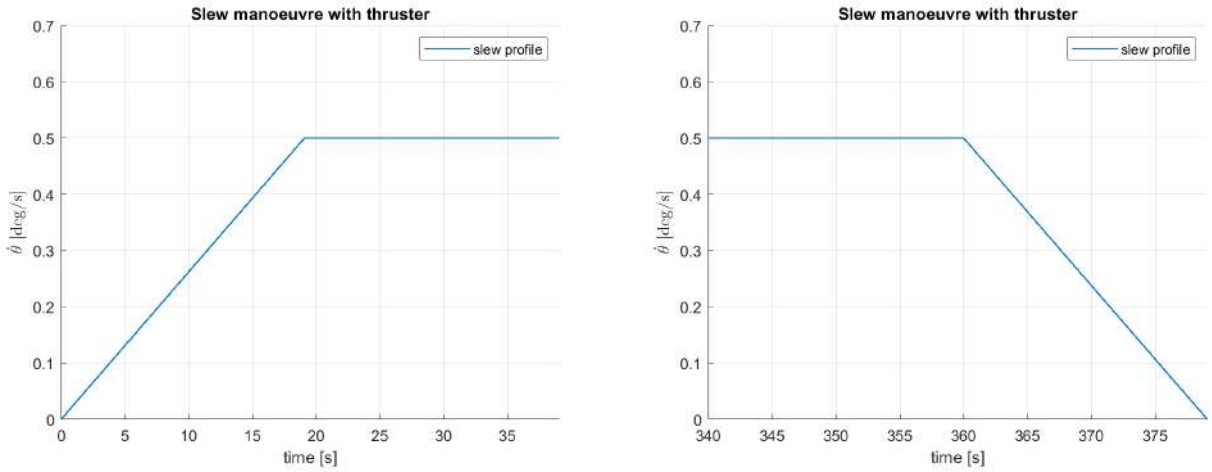

(a) Acceleration phase and initial coasting phase

(b) End of coasting phase and braking phase

Figure 3: Slew maneuvers with thrusters

– Damping Mode: given the knowledge of maximum thrust and the stored angular momentum from the Accumulation Mode of RW, the minimum time of desaturation can be computed:

$$t_{des} = \frac{h_{max}}{nLF_{th_{max}}} = 19.12s \tag{5}$$

The result obtained is equal to the acceleration time and this is due to the fact that the $\dot{\theta}_{acc_{max}}$ depends on the maximum angular momentum stored in the RW, since: Basing on the mission lifetime, that is 4 years by design, and that the orbit period is 1.88 h and accounting the mean deviation angle $\theta = 2.65°$ (in order to obtain a desaturation every 2-3 sols), the total mass of propellant needed to desaturate the RW over the timespan of the PSP can be computed:

$$M_{prop} = \frac{t_{des} n_{des} F}{I_{sp} g_0} = 5.54kg \qquad with \quad n_{des} = 712 \tag{6}$$

2.3 Pointing budget

In table 4 the pointing budgets for different phase are shown:

Control Mode	Task	Solution	Type of Control	Accuracy
Desaturation Mode	Pointing during thrusting	3-axis control	Control using sensors and actuators	AKE, APE 0.3° [2]
Observation Mode	Nadir pointing	3-axis stabilized	Control using sensors and actuators	RPE (3σ) 0.7 mrad (HiRise accuracy)[6]
Communication Mode	HGA pointed towards Earth	2-axis control	Control using gimbals [8]	AKE, APE 2.08 mrad [13]
Power generation Mode	Solar panels pointed to the Sun	2-axis control	Control using 2 gimbals [8]	AKE, APE 1-5 ° (assumed from similar missions) [1]
Slew Maneuvers Mode	Small slew rates	3-axis control	Control using thrusters	$< 0.5\ °/s$
Safe Mode	Pointing towards the Sun during emergencies	3-axis control	Attitude determination using Star trackers, control with RW	$< 5°$

Table 4: Pointing budget

2.4 Mass and Power budgets

In table 5 the mass, power and data budgets per mode of the mission are shown. For the mass budget it was deemed to include also the back-up instruments, since all of them are on-board, even the one that remain unused. Some instrumental data, such as the one for Sun Presence sensors, IMU and Star trackers, are taken from datasheets of instruments used in other space missions, so they might not be entirely accurate. An important clarification shall be provided for the power budget: the data found is in KIPS, Kilo Instruction Per Second, which measures the computer's processor speed [14]. Another important thing to note is that the Data budget, in this case, doesn't depend on how many sensors or actuators are used, but just on the instruction that the on-board computer gives to the instruments.

Control Mode	**Sensors & Actuators used**	**Mass budget (including redundancy)**	**Power budget**	**Data budget** [14]
Desaturation Mode	2 Thrusters [4], 8 Sun Presence sensors [2], IMU [3]	$8 \cdot 1.27 + 16 \cdot 0.005 + 2 \cdot 0.75 = 11.74$ kg	$2 \cdot 8.25 + 8 \cdot 0.13 + 12 = 29.54$ W	$1.2 + 1 + 9 =$ 11.2 KIPS
Observation Mode	8 Sun Presence sensors [2], IMU [3], 3 RW [12]	$16 \cdot 0.005 + 2 \cdot 0.75 + 4 \cdot 9.4 = 39.18$ kg	$8 \cdot 0.13 + 12 + 3 \cdot 17.3 = 64.94$ W	$1 + 9 + 5 = 15$ KIPS
Communication Mode	Gimbal [13], 8 Sun Presence sensors [2], IMU [3]	$45 + 16 \cdot 0.005 + 2 \cdot 0.75 = 46.58$ kg	$14 + 8 \cdot 0.13 + 12 =$ 27.04 W	$15 + 1 + 9 = 25$ KIPS
Power generation Mode	2 Gimbals [13], 8 Sun Presence sensors [2], IMU [3]	$2 \cdot 45 + 16 \cdot 0.005 + 2 \cdot 0.75 = 91.58$ kg	$2 \cdot 14 + 8 \cdot 0.13 + 12 =$ 41.04 W	$15 + 1 + 9 = 25$ KIPS
Slew Maneuvers Mode	2 thrusters [4]	$8 \cdot 1.27 = 10.16$ kg	$2 \cdot 8.25 = 16.5$ W	1.2 KIPS
Safe Mode	2 Star trackers [10], 3 RW [12]	$2 \cdot 0.235 + 4 \cdot 9.4 =$ 38.07 kg	$2 \cdot 1 + 3 \cdot 17.3 =$ 53.9 W	$2 + 5 = 7$ KIPS

Table 5: Budgets per mode

References

[1] Scott D. Benson and Craig R. Tooley. *Long Term Preservation of Mars Express*. Accessed: 26 April 2025. 2006. URL: https://arc.aiaa.org/doi/pdf/10.2514/6.2006-5699.

[2] Fuat Kaan Diriker et al. "Improved accuracy of a single-slit digital sun sensor design for cubesat application using sub-pixel interpolation". In: *Sensors* 21.4 (2021), p. 1472.

[3] Northrop Grumman. "LN-200 FOG Family Advanced Airborne IMU/AHRS". In: ().

[4] Aerojet Rocketdyne Holdings Inc. In: URL: https://satsearch.co/products/aerojet-rocketdyne-mr-106e-28vdc.

[5] Jet Propulsion Laboratory. *MRO Spacecraft Parts: Guidance, Navigation, and Control Systems*. 2006. URL: https://web.archive.org/web/20060331050959/http://mars.jpl.nasa.gov/mro/mission/sc_guide.html.

[6] SW Lee and ED Skulsky. "Mars Reconnaissance Orbiter design approach for high-resolution surface imaging". In: (2003).

[7] Robert E Lock et al. "The Mars reconnaissance orbiter mission plan". In: (2004).

[8] Jet Propulsion Laboratory of NASA. *Spacecraft Parts: Mechanism*. 2008. URL: https://web.archive.org/web/20080418065928/http://marsprogram.jpl.nasa.gov/mro/mission/sc_mechanisms.html.

[9] Lavagna Michéle Roberta. "SSEO-Attitude/orbit determination Control". In: *Politecnico di Milano* (2025).

[10] RocketLab. "ST-16RT2 Datasheet STAR TRACKER High-Performance Star Tracker". In: (2013).

[11] Solar System Exploration Data Services Office. *Mars Reconnaissance Orbiter (MRO)*. Accessed: 26 April 2025. 2024. URL: https://solarviews.com/eng/reconnaissance.htm.

[12] Newspace Systems. *Libra Reaction Wheels*. 2024. URL: https://www.newspacesystems.com/wp-content/uploads/2024/07/Reaction-Wheel-Datasheet-A4-9-1.pdf.

[13] Jim Taylor, Dennis K Lee, and Shervin Shambayati. "Mars reconnaissance orbiter". In: *Deep Space Communications* (2016), pp. 193–250.

[14] J.R. Wertz and W. Larson. *Space Mission Analysis and Design*. Space Technology Library. Springer Netherlands, 1999. ISBN: 9780792359012. URL: https://books.google.it/books?id=QJanyiWfvXMC.

[15] Tung-Han You et al. "Mars Reconnaissance Orbiter interplanetary cruise navigation". In: *Proceedings of the 20th International Symposium on Space Flight Dynamics*. 2007.

[16] Richard Zurek et al. "MRO overview: Sixteen years in Mars orbit". In: *Icarus* 419 (2024), p. 116102.

MRO Reverse Engineering Study

Assignment #5

Team 21

P. Code	Surname	Name
10724393	Chini	Filippo
10721870	Mazzitti	Riccardo
10682521	De Gennaro	Antonio
10764250	Bianco	Emanuele
10668777	Matteotti	Luca
10810285	Basci	Matteo Maria
11076681	Kazenas	Mantas

Space System Engineering and Operations

Prof: M. Lavagna

L. Bianchi, M. Bussolino

M.Sc Space Engineering
A.Y. 2024-2025

Change log	
Issue	*Comments*
1	First release

Contents

1 Design and architecture **1**
1.1 Solutions adopted for the main components of MRO 1
1.2 Link between TCS architecture and operational phases 2

2 Thermal Control System Sizing **3**
2.1 Hot case 3
2.2 Cold case 4
2.3 Conclusions 4
2.4 Insight into Aerobraking phase 5

List of Acronyms	
Acronym	*Full Name*
TCS	Thermal Control System
MLI	Multilayer Insulation
SFC	Spacecraft Flight Computer
SEB	Sharad Electronics Box
RW	Reaction Wheels
HGA	High Gain Antenna
TWTA	Travelling Wave Tube Amplifier
ABX	Aerobraking Phase
EDL	Entry Descent Landing
LPA	Lumped Parameter Approach
CFD	Computational Fluid Dynamics

1 Design and architecture

The Thermal Control Subsystem (TCS) is responsible for maintaining the temperature in all the subsystems of the spacecraft within their respective limits. The main body of the satellite is covered by gold-plated multilayer insulation (MLI) blankets. Their primary function is to reduce excessive heat loss by thermal radiation and are made of Mylar and Kapton sheets with a single layer of aluminized polyamide facing outside and silver aluminum foil facing inside. [5] In the other subsystems, MRO employs several conduction and radiation based techniques for thermal control as: radiators, surface coatings, heaters, and blankets. [18]

1.1 Solutions adopted for the main components of MRO

Solar Arrays The thermal system of the solar arrays shall handle the extreme conditions of Mars orbit, as intense solar heating and deep-space cold and furthermore, shall manage the crucial aerobraking phase. This system relies mainly on passive thermal control, using carefully selected materials and coatings to balance heat absorption and radiation. The panels are built from M55J graphite epoxy composite with an aluminum honeycomb core that provides both stiffness and thermal conductivity. The solar cell side uses high-efficiency $GaInP_2$/GaAs/Ge cells, while the bare side has a coating with $\alpha/\varepsilon \approx 0.89/0.72$, and the cell side has $\alpha/\varepsilon \approx 0.81/0.85$. A Kapton edge layer protects the panel edges from heating.[2]

HiRISE HiRISE employs a tool called HiTemp to model temperatures while HiRISE is operational. It is able to predict temperatures with inputs of HiRISE enviroment and has been found to accurately predict temperatures within 2 °C. This instrument achieves near-zero coefficient of thermal expansion (CTE) by employing graphite-fiber-reinforced composite that have negative CTE alongside metallic positive CTE fittings. The space between primary and secondary mirrors temperature is controlled by heating mats[13]. During operations MRO maintains a uniform temperature of 20 °C of the whole telescope, with an estimate average orbit power consumption of 60 W.[6]

CTX It employs five temperature sensors (Analog Devices AD590), one on the focal plane, two on the electronics board and two on the bakeout heater. All of these sensors are monitored by the Spacecraft Flight Computer (SFC) and not the CTX itself.[22]

MARCI This camera is designed to operate in the temperature range of -35 C to 35 C. Its survival temperature ranges from -80 C to 100 C [17]. In normal operation mode MARCI instrument does not require any additional heat, only time its heat needs to be maintained is when it is powered off.[3]

CRISM CRISM was subdivided into several thermal zones, all of which required different temperatures to operate, thus there was a lot of thought put in thermal control of CRISM instrument. It employed a hybrid approach combining active and passive methods. Actively, it used miniaturized loop heat pipes and heaters to regulate temperatures, ensuring the optics remained near room temperature and the cryocooler-cooled detectors stayed below 110 K. Passive elements included multi-layer insulation (MLI), thermal isolation mounts, and radiators to minimize heat exchange with the spacecraft and Martian environment. Thermal modeling and extensive ground testing were used to predict and control thermal behavior across all mission phases. This robust thermal control system ensured high spectral accuracy and stability, enabling CRISM to operate with near perfect conditions.[15]

SHARAD It is a radar made up of two separate parts: SHARAD electronics box (SEB) and the antenna. SEB is mounted on a support structure, that naturally acts as a radiator and includes

heaters and thermal sensors inside. The antenna on the other hand only employs heaters installed on the spacecrafts panel in order to heat up the antenna cradle hinges in order to keep the actuator mechanism within an suitable temperature range.[21]

Tanks The thermal control system for propellant tanks uses active heaters combined with multi-layer insulation (MLI) to maintain proper temperatures. The tanks need to stay within a narrow temperature range to ensure correct pressurization and prevent freezing or overheating. The MLI reduces heat loss to space, while electrical strip heaters are strategically placed on the tanks to provide supplemental heating as needed. This combination ensures that the tanks remain within operational limits during all mission phases, including the cold cruise and aerobraking periods around Mars.

1.2 Link between TCS architecture and operational phases

The final design of the TCS shall accommodate all the thermal environments encountered since the beginning of the mission until the operational orbit of Mars. The strategy adopted ensures to maintain all the electronics of the satellite in stable conditions for both the hot and cold case. As already mentioned, MRO relies on a classical TCS composed of heaters, radiators, MLI blankets. The scientific payloads are externally mounted and most of them are blanketed and heat to meet their own operating temperature limits. The experiments units perform their own thermal control for the purpose of optimizing the temperature control performances. While the presence of the Sun represents a major heat source that is practically always present (apart from eclipse periods), the heat coming from internal power is minimum during cruise (instruments switched on) and it is maximum during scientific operations (instruments switched on).

Phase	**Thermal fluxes sources**
Launch and Earth departure	Sun radiation, Internal power, Earth albedo, Earth IR radiation
Interplanetary cruise	Sun radiation, Internal power
Aerobraking	Sun radiation, Mars albedo and IR radiation, Atmospheric convection, Internal power
Science operations	Sun radiation, Internal power, Mars albedo and IR radiation
Science operations (in eclipse)	Internal power, Mars IR radiation

Table 1: Main sources of thermal fluxes during the different phases of the mission

Component	**Temperature limits** [°C]
Solar panels	−200, +175 [19]
Antennas	−120, +120
Batteries (Ni-H_2)	−5, +25
Reaction wheels	−20, +50
Star trackers	−10, +120
Propellant tank (N_2H_4)	+5, +50
HiRISE	−110 , +20
CTX	+17, +25
MARCI	−80, +100
CRISM (Spectrometer housing)	−90, −80
SHARAD	−40, +40 (estimation)

Table 2: Temperature ranges for the main components and instruments of the spacecraft [26][14]

2 Thermal Control System Sizing

The sizing of the Thermal Control System is based on two main parameters: the external and internal heat fluxes and the survival temperature range of the spacecraft. The external fluxes have 3 primary sources: the Sun, the albedo due to Mars and the infrared emission of the planet. On the other hand, for the internal flux the main contribution is from the power dissipated by the several instruments on-board.
The range of required temperatures is based on the on-board components survival temperatures; in the case of this report it was deemed the typical temperature range of the RW [26] and it's [-20; 50]°C.
The underlying modeling assumptions of this sizing are the following: steady-state condition, which means that no transient is taken into consideration and that the temperatures are fixed; single-node model, so no multi-nodal analysis was done.
The spacecraft main-body dimensions are $3.5 \times 2.9 \times 2.5$ m, which were taken from bibliography [1] after removing the solar panels and the HGA from the measures.
An iterative process was applied to select the appropriate coating for the spacecraft by testing different materials. The final choice was also influenced by the requirement that the heater provide around 300 W [18], so a metallic coating (bare aluminum) with $\alpha_{sc} = 0.09$ and $\varepsilon_{sc} = 0.085$ was chosen. As can be seen from online images of the MRO spacecraft and its temperature ranges as shown in table 2, the coating surrounds the main body, as this is the part most sensitive by large temperature variations.

2.1 Hot case

For the hot case, the science phase when the Sun is in view was selected, since all the external fluxes are present and most of the instruments are on; this results in the following powers, shown in table 3:

Q_{Sun}	702 W	Q_{albedo}	154 W
Q_{IR}	100 W	Q_{int}^{hot}	592 W

Table 3: Heat and dissipated powers

From this table it can be seen that the powers due to the external heat fluxes aren't that high and that's mostly due to the large distance from the Sun and the low reflectivity of Mars. In order to compute the internal power during the science phase it was necessary to understand which systems and instruments were activated and their relative power consumptions, which are shown in table 4 (for the TWTA and Ka-band the input powers were taken into consideration).

Q_{TWTA}	172 W [24]	Q_{IMU}	12 W [10]
$Q_{Sun\ sensor}$	0.3 W [9]	Q_{RW}	84 W [23]
Q_{HiRise}	60 W [16]	Q_{CTX}	7 W [16]
Q_{Marci}	5 W [16]	Q_{Crism}	46 W [16]
Q_{MCS}	11 W [16]	Q_{Sharad}	20 W
$Q_{Star\ tracker}$	0.5 W [20]	$Q_{Transponder}$	16 W [24]
$Q_{Gimbals}$	42 W [24]	$Q_{Electra}$	71 W [24]
Q_{CPU}	10 W	$Q_{Ka-Band}$	35 W [24]

Table 4: Internal power generation (Sharad and CPU assumed values from similar components)

To be conservative, it was decided that all the power generated would be convert in heat power. The total internal power is computed:

$$Q_{\text{payload}} = Q_{\text{HiRise}} + Q_{\text{CTX}} + Q_{\text{Marci}} + Q_{\text{Crism}} + Q_{\text{MCS}} + Q_{\text{Sharad}} = 149W \tag{1}$$

$$\begin{aligned} Q_{\text{int\_hot}} = {} & Q_{\text{TWTA}} + Q_{\text{payload}} + Q_{\text{Imu}} + Q_{\text{startrack}} + Q_{\text{sunsens}} + \\ & Q_{\text{RW}} + Q_{\text{transp}} + Q_{\text{gimbals}} + Q_{\text{electra}} + Q_{\text{CPU}} + Q_{\text{Kaband}} = 592W \end{aligned} \tag{2}$$

From these data it is possible to retrieve the T_{hot} in an uncontrolled case. With this type of coating chosen, the value found is:

$$T_{hot} = 34.2°C < 35°C = T_{max\ margined} \tag{3}$$

From this result, it is possible to understand that radiators are not needed since the condition is satisfied and no power has to be dissipated, so the passive action of the coating is enough to remain in the temperature range. The fact that the spacecraft is not equipped with radiators in the calculations is not surprising, since Mars missions are characterized by much lower solar heat input compared to those to planets closer to the Sun.

2.2 Cold case

In this case the spacecraft is sized while in eclipse, with the payload turned off, since the instruments can't work without sunlight, and with only the TWTA turned on regarding the telecommunication system. Here in table 6 the values used are shown:

Q_{IR}	100 W	Q_{int}^{cold}	391.5 W

Table 5: Heat and dissipated powers

In the same way as it was done in the Hot case it is possible to evaluate the internal power generated during this phase:

$$Q_{\text{int\_cold}} = Q_{\text{TWTA}} + Q_{\text{Imu}} + Q_{\text{startrack}} + Q_{\text{RW}} + Q_{\text{gimbals}} + Q_{\text{electra}} + Q_{\text{CPU}} = 368.5W \tag{4}$$

Now is possible to derive the temperature of the spacecraft in an uncontrolled case:

$$T_{cold} = -45°C < -5°C = T_{min\ margined} \tag{5}$$

The condition $T_{cold} > T_{min\ margined}$ is not satisfied, so it is necessary to add heaters that permit to satisfy the temperature limits. The minimum power requested by the heaters (considering also an addition of 25% margin) is $Q_{heat} = 505$ W supplied by an area of $A_{heat} = 1.625\ m^2$.

2.3 Conclusions

The electric power needed for the heaters obtained by this sizing is higher than the one found in literature (300 W [18]); this difference can be explained by the simplifying assumption that was made at the beginning of the sizing: the mono-nodal analysis. Most certainly the original spacecraft design included a multi-nodal analysis, that offers a more realistic assessment of the thermal gradients of the spacecraft since different nodes are defined to represent the most critical points to monitor in terms of temperature gradient.
Despite this discrepancy, the value computed for the electric power required for the heaters was considered feasible, since MRO has a maximum electrical output of 2000 W, which is enough to sustain both this power and all the other ones from the turned on instruments simultaneously.

A further difference between the sizing presented and the real mission is the absence of the radiators. The temperature range of the actual mission couldn't be found, but it's safe to assume that it was more stringent than the one taken into consideration in this report, leading to a more complex thermal control that included the radiators.
Another factor to note is the coating, which shall be applied all over the main body shell, since that's where all the most thermally sensible instruments are located. As stated previously, after an iterative process, it was concluded that the bare Aluminum coating was the best option for our computations, since it had low values of absorptivity and emissivity, which were necessary in order to have a feasible extreme temperatures range since the values of the external heat fluxes, and consequentially of the maximum and minimum temperatures reached, are strictly related to them. However, MRO has a different type of passive temperature control, which is based on gold-plated multilayer blankets made of Mylar and Kapton sheets; this dissimilarity is due to the simplifying assumptions made regarding the modeling of the spacecraft (mono-nodal) and the temperature range taken into consideration (RW survival temperature range).
The final remark that has to be made regards how the thermal protections that have been sized shall be located in the spacecraft. Since all the more sensitive components are mounted in the main body, the coating shall be applied around it. The exact locations of the heaters inside the spacecraft are not well documented in the literature. However, it has been surmised that the heaters are primarily located in the upper part of the spacecraft, because the main payloads (like CRISM) are situated in the lower part and require operation within a narrow, low-temperature range.

2.4 Insight into Aerobraking phase

The aerobraking phase (ABX) is the most critical phase for solar panels because they shall bear much incoming heat transfer rate from stagnation flow. First and foremost, the ABX heat flux shall be properly assessed at a preliminary design phase, and, moreover, the walk-in phase is modeled as a single maneuver at the apoapsis of the post-MOI capture orbit to lower the periapsis to 100 km, so that the spacecraft dips at the maximum anticipated speed. The largest ABX heat flux can be computed as follows by choosing $c_H = 0.8$: [11]

$$q_{ABX} = \frac{1}{2} c_H \rho v^3 \tag{6}$$

Such a contribution in the actual mission shall outgrow the remaining heat fluxes, because of the high relative velocity in the Martian upper atmosphere, whose composition is 95.37% in carbon dioxided and 5.43% in nytrogen.

$M_{m;\,atm}$	$0.0433\,\mathrm{kg\,mol^{-1}}$ [12]	$T_{inf;\,free\ stream}$	$144.7\,\mathrm{K}$ [11]
$T_{dissociation}$	$2500\,\mathrm{K}$	v_{inf}	$4.8\,\mathrm{km\,s^{-1}}$ [4]
$t_{ABX;\,pass}$	$250\,\mathrm{s}$	ρ	$1\,\mathrm{kg\,km^{-3}}$
q_{ABX}	$44.2368\,\mathrm{W\,m^{-2}}$	Ma	9.88
a	$0.0039\,\mathrm{W/m^4}$	b	$0.5898\,\mathrm{W/m^3}$
ϵ_{panel}	0.35	α_{panel}	0.35
$\rho_{panel} = \frac{M}{A\sum_{i=1}^{5} th_i}$	$174.7256\,\mathrm{kg/m^3}$	c_{panels}	$900\,\mathrm{J/kgK}$

Table 6: Datas and results for ABX phase

The mass was considered 48 kg [7], layers' thickness were taken from [8], area was computed from the size of solar panels [1], while the specific heat was assumed at $900\frac{J}{kgK}$ for simplification, that is that of Aluminum Honeycomb. Of relevant importance to point out is the assumption on the maximum

total temperature because there is dissociation that ceils the total temperature and 2500-3000 K range is typically employed for rough estimations. Such assumption on the maximum temperature limits the Mach number at 9.88. Also the density was considered fairly low against the much higher values in the literature [25], because Martian atmospheric density is highly prone to variation in time and in altitude and because the computation of the density from orbit propagation plus density-altitude exponential model was not covered in this analysis. Moreover the effective time accounted for the ABX simulation is 250 s, lower than the 500 s from the literature graphs [19], yet because the density is considerably low at the onset of the ABX pass. The heat flux, thereby the convective heat transfer between the solar panels wall and the flow, is interpolated as two branches of parabola within the ABX pass, while the general conduction equation with LPA is applied to trace the temperature evolution at the external wall:

$$a = \frac{8q_{ABX}}{t_{ABX}^2} \tag{7}$$

$$b = \frac{4q_{ABX}}{t_{ABX}} \tag{8}$$

$$q(t) = \frac{1}{2}at^2, \mathrm{t} < \frac{t_{ABX}}{2} \tag{9}$$

$$q(t) = q_{ABX} - b(t - \frac{t_{ABX}}{2}) + \frac{a}{2}(t - \frac{t_{ABX}}{2})^2, \frac{t_{ABX}}{2} < t < t_{ABX} \tag{10}$$

$$\rho_{panel} c_{panel} V_{panel} \frac{\partial T}{\partial t} = -q(t)(T(t) - T_{dissociation}) - \sigma \epsilon_{panel} A_{panel}(T(t)^4 - T_{space}^4) \tag{11}$$

The maximum temperature reached is 180°C, which breaches the 20°C margined result of 175°C in literature [19]. However, it is important to underscore that such a simulation relied on assumption of a low atmospheric density and a two-branch parabola trend over time for the heat flux, which is a fairly conservative approach, and that scaling the atmospheric density up of an order of magnitude might yield unforbidden maximum temperatures of over 1000°C and, nonetheless, the LPA faults in any case for high atmospheric densities because the Biot number becomes larger than 0.1. Therefore a more precise CFD model is entailed to properly assess the actual temperature distribution over the solar panels along with a precise orbital path simulation with drag and J2. Given the peak temperature during ABX, proper passive thermal control shall be entailed and the spacecraft attitude shall be properly controlled so as not to damage the solar panels. Moreover, given each drag pass is a transient phase, those were discarded as a potential candidate for the hot case for the main body, because that is properly ensembled in MLI blankets, which shall effectively deplete the strong heat fluxes over the aerobraking phase.

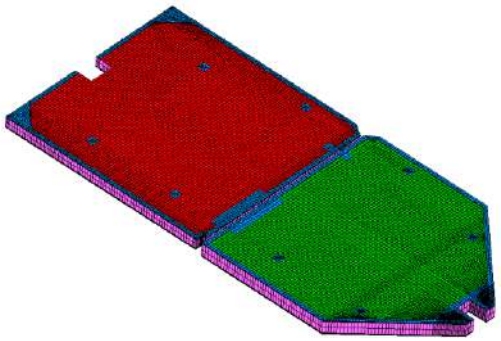

Figure 1: Solar Array

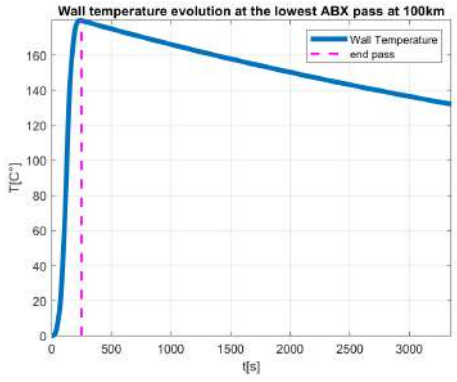

Figure 2: Wall temperature trend with backward Euler Method

References

[1] NATIONAL AERONAUTICS and SPACE ADMINISTRATION. *Mars Reconnaissance Orbiter Launch*. August 2005. URL: https://www.jpl.nasa.gov/news/press_kits/mro-launch-Aug05.pdf.

[2] Ruth M. Amundsen, John A. Dec, and Joseph F. Gasbarre. "Thermal Model Correlation for Mars Reconnaissance Orbiter". In: *37th International Conference on Environmental Systems (ICES)*. Chicago, IL, USA: NASA Langley Research Center, July 2007. URL: https://ntrs.nasa.gov/citations/20070030304.

[3] J.-P. Bibring et al. "Mars surface diversity as revealed by the OMEGA/Mars Express observations". In: *Journal of Geophysical Research: Planets* 114.E00D08 (2009), E00D08. DOI: 10.1029/2008JE003315. URL: https://agupubs.onlinelibrary.wiley.com/doi/full/10.1029/2008JE003315.

[4] AM Brandis. *Updated Stagnation Point Aeroheating Correlations for Mars Entry*. Tech. rep. 2018.

[5] Emilie Brannan. "Thermal Control and Heating System in Space". PhD thesis. Nov. 2020. DOI: 10.13140/RG.2.2.36279.34723.

[6] J. van Casteren et al. "BepiColombo - A Mission to Mercury". In: *55th International Astronautical Congress*. Vancouver, Canada, 2004. DOI: 10.2514/6.IAC-04-Q.3.B.02. URL: https://arc.aiaa.org/doi/pdf/10.2514/6.IAC-04-Q.3.B.02.

[7] John A Dec, Joseph F Gasbarre, and Ruth M Amundsen. *Thermal Modeling of the Mars Reconnaissance Orbiter's Solar Panel and Instruments During Aerobraking*. Tech. rep. SAE Technical Paper, 2007.

[8] Alessandro DiCarlofelice et al. "A new numerical model of the HF antenna of the Mars Reconnaissance Orbiter's (MRO) Shallow Radar (SHARAD) and first results from a test at a high-angle spacecraft roll". In: *Icarus* 419 (2024), p. 115802.

[9] Fuat Kaan Diriker et al. "Improved accuracy of a single-slit digital sun sensor design for cubesat application using sub-pixel interpolation". In: *Sensors* 21.4 (2021), p. 1472.

[10] Northrop Grumman. "LN-200 FOG Family Advanced Airborne IMU/AHRS". In: ().

[11] Derek S Liechty. "Aeroheating analysis for the Mars reconnaissance orbiter with comparison to flight data". In: *Journal of Spacecraft and Rockets* 44.6 (2007), pp. 1226–1231.

[12] Professor Maggi. *Space Propulsion lecture slides "LRM"*.

[13] A.S. McEwen et al. "The high-resolution imaging science experiment (HiRISE) in the extended science phase". In: *Icarus* 401 (2024), p. 115388. DOI: 10.1016/j.icarus.2023.115388. URL: https://www.sciencedirect.com/science/article/pii/S0019103523003731.

[14] Lucia Bianchi Michèle Roberta Lavagna Massimiliano Bussolino. "Exercise session". In: *Polimi* (2025).

[15] S. L. Murchie et al. "Compact Reconnaissance Imaging Spectrometer for Mars (CRISM) on Mars Reconnaissance Orbiter (MRO)". In: *Journal of Geophysical Research: Planets* 112.E05S03 (2007). DOI: 10.1029/2006JE002682. URL: https://agupubs.onlinelibrary.wiley.com/doi/full/10.1029/2006JE002682.

[16] NASA. *Mars Reconnaissance Orbiter Science Instruments*. URL: https://science.nasa.gov/mission/mars-reconnaissance-orbiter/science-instruments/.

[17] NASA. *NASA Space Science Data Coordinated Archive*. URL: https://nssdc.gsfc.nasa.gov/nmc/experiment/display.action?id=1998-073A-01.

[18] NASA. *Thermal Systems*. Accessed: 2025-05-09. 2015. URL: https://web.archive.org/web/20150905185258/http://mars.nasa.gov/mro/mission/spacecraft/parts/thermal/.

[19] Jill L Prince, John A Dec, and Robert H Tolson. "Autonomous aerobraking using thermal response surface analysis". In: *Journal of Spacecraft and Rockets* 46.2 (2009), pp. 292–298.

[20] RocketLab. "ST-16RT2 Datasheet STAR TRACKER High-Performance Star Tracker". In: (2013).

[21] R. Seu et al. "SHARAD sounding radar on the Mars Reconnaissance Orbiter". In: *Journal of Geophysical Research: Planets* 112.E05S05 (2007). DOI: 10.1029/2006JE002745. URL: https://agupubs.onlinelibrary.wiley.com/doi/full/10.1029/2006JE002745.

[22] A. Spiga and F. Forget. "Remote sensing of surface pressure on Mars with the Mars Express/OMEGA spectrometer: 2. Meteorological maps". In: *Journal of Geophysical Research: Planets* 112.E8 (2007), E08S16. DOI: 10.1029/2006JE002808. URL: https://agupubs.onlinelibrary.wiley.com/doi/full/10.1029/2006JE002808.

[23] Newspace Systems. *Libra Reaction Wheels*. 2024. URL: https://www.newspacesystems.com/wp-content/uploads/2024/07/Reaction-Wheel-Datasheet-A4-9-1.pdf.

[24] Jim Taylor, Dennis K Lee, and Shervin Shambayati. "Mars reconnaissance orbiter". In: *Deep Space Communications* (2016), pp. 193–250.

[25] R Tolson et al. "Atmospheric modeling using accelerometer data during Mars Reconnaissance Orbiter aerobraking operations". In: *Journal of Spacecraft and Rockets* 45.3 (2008), pp. 511–518.

[26] J.R. Wertz and W. Larson. *Space Mission Analysis and Design*. Space Technology Library. Springer Netherlands, 1999. ISBN: 9780792359012. URL: https://books.google.it/books?id=QJanyiWfvXMC.

MRO Reverse Engineering Study

Assignment #6

Team 21

P. Code	Surname	Name
10724393	Chini	Filippo
10721870	Mazzitti	Riccardo
10682521	De Gennaro	Antonio
10764250	Bianco	Emanuele
10668777	Matteotti	Luca
10810285	Basci	Matteo Maria
11076681	Kazenas	Mantas

Space System Engineering and Operations

Prof: M. Lavagna

L. Bianchi, M. Bussolino

M.Sc Space Engineering
A.Y. 2024-2025

Change log	
Issue	*Comments*
1	First release

Contents

1 EPS Design and Architecture **1**
1.1 Solar Panels . . . 1
1.1.1 Structure of the panels . . . 1
1.2 Batteries . . . 1
1.3 Electrical Power and Energy Requirements by Mission Phase . . . 2

2 Sizing **3**
2.1 Power Budget . . . 3
2.2 Solar Array sizing . . . 4
2.3 Battery sizing . . . 5

List of Acronyms	
Acronym	*Full Name*
EPS	Electric Power System
TMTC	Telecom & Telemetry System
PS	Propulsion System
ADCS	Attitude Determination & Control System
RW	Reaction Wheels
HGA	High Gain Antenna
TCS	Thermal Control System
OBDH	On-Board Data Handling
SA	Solar Array
IMU	Inertial Measurement Unit
DET	Direct Energy Transfer
EoL	End of Life
BoL	Beginning of Life
MJD	Modified Julian Date

1 EPS Design and Architecture

The Electric Power System (EPS) that is present in the MRO is responsible for generating, storing, and distributing power to all subsystems and scientific payloads onboard. This system is divided into two components: two solar panels and two batteries. The solar arrays has been sized to fulfill the requirement to support operations of all instruments in the different Mars seasons. An important characteristic of observations is the ability to have power that all the instruments can be powered on, whether the spacecraft is at perihelion or aphelion. Thus, scientific campaigns can continue almost concurrently in every orbit.[12]

1.1 Solar Panels

Since the only primary source of power for MRO is the light of the Sun, two panels are mounted on opposite sides of the spacecraft. As soon as the spacecraft was clear of the launch vehicle, the orbiter deployed its solar arrays to begin producing power, and they have remained deployed throughout the mission.[12] The spacecraft is equipped with two gimbaled connections that allow the arrays to track the Sun as MRO coasts around Mars each orbit. This functionality allows both solar arrays point to sun, while the antenna is pointing to earth and science instruments to martian surface[14]. In some cases, targeting requires rolling the spacecraft up to 30° off-nadir and these rolls affect power generation because the panels are not at their best position relative to the Sun for even 20 minutes.[23] Each panel has an area of about $10\,m^2$ ($20.5\,m^2$ combined) and contains 3744 solar cells. These high-efficiency cells convert more than 26% of the energy into electricity and, since they are connected together, the power produced is 32 volt. When orbiting Mars, the panels together generate 2000 watts of power at the start of the science phase, whereas they would generate 6000 W in a comparable Earth orbit by being closer to the Sun.[12][13]

1.1.1 Structure of the panels

The MRO has a main bus made of titanium, carbon, and aluminum honeycomb; two solar panel wings extend from this main bus structure. [11] The MRO solar array comprises five distinct layers: two composite facesheets, a solar cell layer, an aluminum honeycomb core and a Kapton layer.
The multi-layer configuration ensures the structural strength and Mars-specific operational thermal requirements. The model also included variable thicknesses of facesheets and core for both inboard and outboard sections, as well as variable densities and thicknesses at hard points and hinge connections. This tailored approach balanced the solar array's performance: sustaining launch load expectations and enduring thermal operational stress while remaining lightweight. In addition, edge protection is provided by a Kapton layer that wraps each array section at its outer circumference. [6]
The solar arrays represent a significant engineering solution for the mission's power needs since the as-built mass of the MRO solar array is 48.3 kg, which is approximately 4.7% of the spacecraft's dry mass. The Phased construction incorporated multilayer composite facing sheets and an aluminum honeycomb core which provided exceptional strength to weight ratios while meeting thermal management requirements. The arrays were designed with a slight mass margin, where model mass of 47.5kg and as built 48.3kg representing a 1.6 percent difference, portraying careful design to ensure optimal performance while providing operational buffers. [6] [11]

1.2 Batteries

The MRO satellite batteries supply the needed electrical power for the mission during the dark or sunless periods as the MRO travels "behind" Mars during each two-hour orbit and the spacecraft's solar panels are not exposed to sunlight. The batteries are then recharged each time the MRO sees the sun owing to the electricity produced by the solar cells. At Mars arrival, 21 minutes into the burn, the MRO passed into the shadow of the planet and its EPS switched the electric power source from the solar panels to the spacecraft's batteries. Two

nickel-hydrogen rechargeable batteries are exploited by MRO and each one has a storage capacity of 50 A h at 32 V that translates in 1600 W for one hour. For safety reasons, only about 40% of the battery capacity is ever planned to be used because as a battery discharge, the voltage drops and if it drop below 20 V the on-board computer would stop functioning [12]. In fact, the batteries full capacity was forcefully constrained in order to save its life time that is more valuable during long-term space missions. In the event that the voltage drops bellow 20 Volt it would not be able to maintain power supply to the flight computer. [12]

1.3 Electrical Power and Energy Requirements by Mission Phase

The primary challenge in designing MRO's solar array during the aerobraking phase was thermal control, as exposed components generated significant heat. Analysis showed that the solar array faced the most stringent thermal constraints throughout this phase, with less margin compared to the scientific instruments, based on the Engineering Requirements Document.[6]
The thermal limits for the solar array were primarily determined by the peak heat flux encountered and the length of the drag pass (i.e., the total heat load). [6] During the aerobraking segment, the power generation capability of the solar array was likely reduced due to thermal constraints and suboptimal solar panel orientation. Power management during aerobraking required careful balancing of orientation for both drag and power generation.[6]
The solar panels were not permanently orthogonal to the Sun direction, but their orientation varied significantly depending on mission phase and operational constraints During normal science operations, typical Sun incidence angle was <5 from perpendicular, meanwhile during aerobraking phase the panels were angled up to 60° from Sun direction to reduce atmospheric drag torque and limit thermal loads during atmospheric passes. The observed minimum operational angle was 60° during peak aerobraking, reducing solar flux to 50% but still allowing partial power generation while managing thermal loads. [7] For the science mission phase, each scientific instrument had specific power requirements that the Electrical Power System (EPS) needed to meet. These instruments require stable, continuous power to carry out their scientific observations throughout the extended mission.
Effect of Solar Distances: Mars' distance from the Sun will always lead to reduced Solar intensity when compared to Earth. This requires solar panels to be larger in size than what is required for Earth-orbiting missions.[19]

Thermal Environment Control: For solar, thermal arrays management during cooling is a critical factor. During the aerobraking phase, these temperatures were monitored and controlled to avoid breaching the allowable temperature of 175C. This constraint had a direct influence on operation and power production capacity.[6]

Considerations of Aspect Angle: While not precisely outlined in the search results, MRO would need to manage solar array pointing to aspect angle requirements for balancing power generation to the science requirements for lower altitude observations and the thermal limits. The most stringent aerospace-vehicle thermal interactions occur during solar aerobraking. From the comparison of the solar array thermal limit line to the solar ERD, it can be noticed that for drag durations of 300-1500 seconds, the maximum allowable heat flux reduces from approximately 0.65 watts per cm squared to 0.30 watts per cm squared. This phenomenon where the drag duration relates directly to heat flux had to be figured out in mission operations and power management for main propulsion during these critical phases of the mission.

2 Sizing

2.1 Power Budget

In order to size the EPS, the first thing to do is the power budget, which consists of analyzing how much electrical power each subsystem needs in each mode during science phase and the results are shown in the following tables:

SUBSYSTEM POWER	COMMUNICATION [W]	MANEUVER [W]	OBSERVER MODE [W]	ECLPISE [W]
PS	/	109.8	/	/
ADCS	138.3	124.3	124.3	96.5
TMTC	223	16	16	16
TCS	279	279	279	300
Others (EPS, OBDH,...) (estimation)	100	100	100	100
PAYLOAD	98.6	36.1	220	139
TOTAL	838.9	665.1	739.3	651.5
+20 % margin	167.8	133	147.9	130.3
TOTAL MARGINED	1006.6	798.2	887.2	781.8

It can be seen that the mode that requires more power in sunlight is the communication mode, mainly due to the high input powers of the TMTC subsystem. Here follows the power budget for each component and payload:

COMPONENTS	COMMUNICATION [W]	MANEUVER [W]	OBSERVER MODE [W]	ECLPISE [W]
Thrusters (8) [8]	/	109.8	/	/
IMU [5]	12	12	12	12
Gimbals SA (2) [22]	28	28	28	/
Gimbal HGA [22]	14	/	/	/
Sun sensors (8) [2]	0.3	0.3	0.3	/
Star tracker [20]	/	/	/	0.5
RW (3) [21]	84	84	84	84
X-band [22]	172	/	/	/
Ka-band [22]	35	/	/	/
Transponder [22]	16	16	16	16
Cryocoolers (3) [17]	69	69	69	/
Heaters [3]	210	210	210	300

It can be observed that the HGA and the solar arrays need to perform precise pointing for power generation and communication with Earth respectively, so gimbals that carry out this task according to the mode are necessary.

For each payload it was considered a 12% of power usage in sleep mode, this hypothesis is based on the fact that Electra consumes the 12% of power even if not used [10], so the same has been assumed for all the other payloads.

PAYLOADS	COMMUNICATION [W]	MANEUVER [W]	OBSERVER MODE [W]	ECLPISE [W]
Electra [22]	71	8.5	71	71
MCS [15]	11	11	11	11
Sharad [15]	2.4	2.4	20	2.4
MARCI [15]	0.6	0.6	5	0.6
CRISM [15]	5.5	5.5	46	5.5
HiRise [15]	7.2	7.2	60	7.2
CTX [15]	0.8	0.8	7	0.8

2.2 Solar Array sizing

The primary source of power of MRO are the solar arrays, which need to produce enough power to make the spacecraft operational. After studying the various power budgets per mode, in order to size the solar panels, the power requested in sunlight and eclipse are taken; in this case the sunlight mode corresponds to the communication mode, since that's the one that consumes more power. The power of the solar arrays is a function of the powers requested in sunlight and eclipse, the sunlight and eclipse time and the lines efficiency, which in turn depends on the type of power control. Even though no reliable information was found regarding this argument, it was assumed that MRO uses a DET, Direct Energy Transfer, power control since it's the usual configuration for this type of missions due to its simplicity, also no data about the ability of adjusting the solar array's voltage was found, suggesting that no Peak Power Tracking configuration was used. The following values have been used for the sizing:

P_e	781.8 W	P_s	1006.6 W
T_e	40 min	T_s	73 min
X_e	0.85	X_s	0.65

Table 1: Initial data

From these values the power to be produced by the solar arrays can be computed:

$$P_{sa} = \frac{\frac{P_e T_e}{X_e} + \frac{P_s T_s}{X_s}}{T_s} = 1845W \tag{1}$$

To compute the area of solar arrays required, it's necessary to calculate the beginning and end of life power output:

ε	0.3	I_d	0.5
dpy	0.03	$years$	4
p_{BoL}	88.8 W/m^2	p_{EoL}	78.6 W/m^2

Table 2: Output power at beginning and end of life

The area and the number of cells of the solar arrays can then be computed, $A_{sa} = 23.47\ m^2$ and $N_{cells} = 7777$, but, due to the fact that the electrical parameters of the solar arrays should be the same of the system one, the number of cells in series ($N_{series} = 14$) and in parallel ($N_{parallel} = 557$) can also be computed, knowing the system voltage ($V_{sys} = 32\ V$ [12]). This value is considered constant, since a fully regulated configuration was chosen regarding the bus power regulation. From these two parameters, the real number of cells and the real area can be obtained, $A_{sa,real} = 23.53\ m^2$ and $N_{cells,real} = 7798$, from which the total power at the beginning and end of life can be estimated: $P_{BoL} = 2089.5\ W$ and $P_{EoL} = 1850\ W$.
Finally, given the specific power of the solar arrays 80 $\frac{W}{kg}$ (GaInP/GaAs/Ge (3J) [9]), the mass of the sum of the solar cells can be measured, $M_{cells} = \frac{P_{real,BoL}}{SpecificPower} = 26.12\ kg$. It's important to understand that this value computed only takes into consideration the mass of the sum of the solar cells, not of any other possible components of the solar arrays such as cables.
The values obtained are similar to the real mission one found in literature, especially for the total power and the solar array area, suggesting that the initial hypothesis and values chosen for the subsystems electric output are valid and correspond, at least for a majority, to the one of MRO. The area of solar cells obtained is quite high but it can be divided into two solar arrays with dimensions $5.35 \times 2.20\ m$, which are similar to the areas of the real mission panels ($5.35 \times 2.53\ m$ [1]). Doing so has several benefits:

- **better attitude control**, since having two symmetrical panels allows for balancing the torques generated by the external disturbances, such as SRP;
- **better solar efficiency**, thanks to the control mechanisms for each panel that lets the single panels follow better the position of the Sun;
- **redundancy**, if one of the panels malfunctions or breaks, the other one will still be able to produce at least half the power needed.

2.3 Battery sizing

The secondary power source on MRO are the NiH_2 batteries, whose main functionality is to supply the spacecraft with power in eclipse mode. The batteries' sizing only requires the knowledge of the power in eclipse, because the payloads for imaging shall be mantained functional in idling mode and the heaters shall receive maximum power to heat up the entirety of the spacecraft. First and foremost, the energy each battery shall store can be computed:

$\boldsymbol{DoD}$	0.4 [16]	$\boldsymbol{\eta}$	0.7 [9]
$\boldsymbol{V_{batt;cell}}$	1.175 V [18]	$\boldsymbol{\mu}$	0.8 [9]
$\boldsymbol{C_{cell}}$	50 Ah [16]	$\boldsymbol{N_{batteries}}$	2 [4]
$\boldsymbol{E_{wh}}$	$50\frac{Wh}{kg}$ [19]	$\boldsymbol{E_{\rho}}$	$55\frac{Wh}{lt}$ [19]

Table 3: Batteries' sizing datas

$$E_{battery} = \frac{P_{eclipse}T_{eclipse}}{X_e \eta N_{batteries} DoD} \tag{2}$$

As illustrated in the solar panels cells' sizing, the constant system voltage ($V_{sys} = 32V$) shall be considered to determine the number of cells in series in the light of the fully regulated configuration for the bus. The capacity of each battery depends on the DoD and the efficiency at the end of life, along with the power supplied at eclipse phase and the nominal eclipse timespan. Set the voltage batteries, the topology ($N_{cell;series}$, $N_{cell;//}$) can be assessed, thus in turn the maximum available energy from the pack and the actual batteries' capacity.

$N_{cell;series} = \frac{V_{sys}}{V_{batt;cell}}$	28	$E_{string} = \mu C_{cell} V_{batt;cell} N_{batt;series}$	1316 Wh
$N_{cell;//} = ceil(\frac{E}{E_{string}})$	2	$N_{cell} = N_{cell;series}(N_{cell;//} + 1)$	74
$E_{pack} = E_{string} N_{cell;//}$	3948 Wh	$C_{batt;real} = \frac{E_{pack}}{N_{batteries} V_{sys}}$	61.69 Ah
$M_{battery}$	71.78 kg	$\upsilon_{batt} = \frac{E_{pack}}{E_d}$	78.96 lt

Table 4: Batteries' sizing workflow

It is evident a couple of strings suffices for the pack because of the significantly high capacity of a single cell, which also translates into a real capacity quite similar to the original one. Also the real storable energy by a single battery, which is 1974Wh, is scaled accordingly. The knowledge of the energy density and the specific energy from the materials of the batteries sets the basis for the estimation of the mass and the volume of the pack. At first glance, those computed values are quite realistic because the pack shall not take up much of space and weight when considering the spacecraft as a whole. However, given the pack's weight ($> 70kg$) being higher than that of critical components such as solar panels and HGA, and comparable to the on-board imaging payloads, and because the thermal blankets ensure proper shielding against solar radiation and grant thermal insulation, the pack shall be placed off the main body's geometric center, slightly left-down from the viewpoint of the face where roll axis points inward, for several reasons:

- to bridge as much as possible the gap between the roll inertia and pitch inertia, thus to shrink the instability margin on account of the Gravity Gradient, leveraging coupling effects in the inertia matrix;
- to avoid interwoven routings;
- for vicinity to thermally sensitive payloads, like HiRISE and and CTX, in order to minimise cable losses owing to the Joule effect and, therefore, to effectively heat up the envelopes and to cool down the lens.

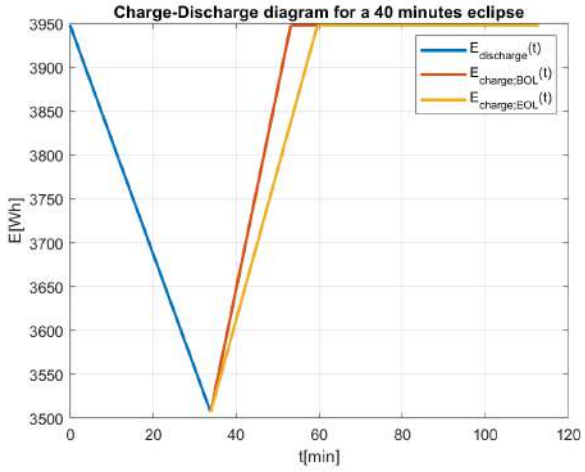

Figure 1: Charge-discharge diagram: BoL: 6-10-2006 and EoL:10-7-2010

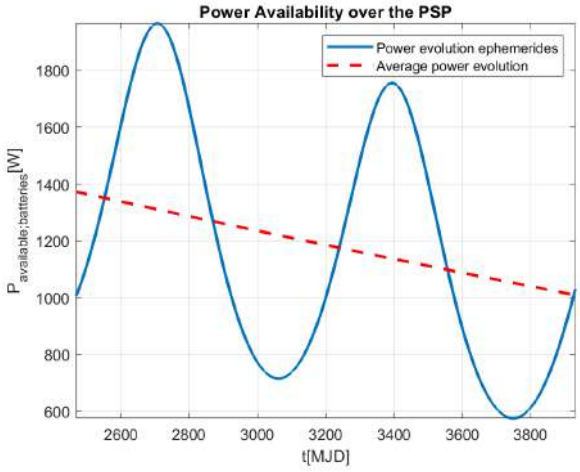

Figure 2: Power availability for the battery pack: BoL: 6-10-2006, EoL: 10-7-2010

As shown in Figure 1, 2 full martian orbits were accounted in for to draw a clear comparison at specific distance from the Sun, which for the plot is 1.63AU at BoL and EoL MJD dates. Moreover, in the sizing, with a mission timespan of 4 years, the discharge level of the battery never drops below 10-11% because the cell implemented for the battery pack has a large capacity of 50Ah.

$$P_{\text{available}}(t) = \frac{1-\epsilon}{\epsilon} \cdot X_e \cdot \left(P_{\text{BOL}}(t) \cdot (1 - dpy)^{(t-t_0)} - \frac{P_s}{X_s} \right) \tag{3}$$

References

[1] NATIONAL AERONAUTICS and SPACE ADMINISTRATION. *Mars Reconnaissance Orbiter Launch*. August 2005. URL: https://www.jpl.nasa.gov/news/press_kits/mro-launch-Aug05.pdf.

[2] Fuat Kaan Diriker et al. "Improved accuracy of a single-slit digital sun sensor design for cubesat application using sub-pixel interpolation". In: *Sensors* 21.4 (2021), p. 1472.

[3] Wikipedia France. *Mars Reconnaissance Orbiter, Caractéristiques techniques de la sonde spatiale, Protection thermique*. URL: https://fr.wikipedia.org/wiki/Mars_Reconnaissance_Orbiter.

[4] James E Graf et al. "The Mars reconnaissance orbiter mission". In: *Acta Astronautica* 57.2-8 (2005), pp. 566–578.

[5] Northrop Grumman. "LN-200 FOG Family Advanced Airborne IMU/AHRS". In: ().

[6] Ruth M. Amundsen John A. Dec Joseph F. Gasbarre. "Thermal Modeling of the Mars Reconnaissance Orbiter's Solar Panel and Instruments During Aerobraking". In: *Proceedings of the 37th International Conference on Environmental Systems (ICES)*. Paper No. 07ICES-64. Chicago, Illinois, USA, July 2007. URL: https://ntrs.nasa.gov/api/citations/20070029236/downloads/20070029236.pdf.

[7] Justin Kerr, John E. Moores, and Christina L. Smith. "An improved model for available solar energy on Mars: Implications for power generation on the surface". In: *Advances in Space Research* 72.6 (2023), pp. 1431–1445. DOI: 10.1016/j.asr.2023.06.013. URL: https://ui.adsabs.harvard.edu/abs/2023AdSpR..72.1431K/abstract.

[8] Robert E Lock et al. "The Mars reconnaissance orbiter mission plan". In: (2004).

[9] Lucia Bianchi Michéle Lavagna Massimiliano Bussolino. "Exercise: Electrical Power System, Solar array sizing". In: (2025).

[10] NASA. *Mars Exploration Program, Electra Mars Proximity-Link Communications and Navigation Payload Description*. URL: https://discovery.larc.nasa.gov/PDF_FILES/29Electra_Description.pdf.

[11] NASA. *Mars Reconnaissance Orbiter*. https://science.nasa.gov/mission/mars-reconnaissance-orbiter/. Accessed: 2025-05-15. 2025.

[12] NASA. *Mars Reconnaissance Orbiter – Electrical Power*. https://web.archive.org/web/20221206092503/https://mars.nasa.gov/mro/mission/spacecraft/parts/electricalpower/. Accessed: 2025-05-15. 2022.

[13] NASA. *Mars Reconnaissance Orbiter Arrival Press Kit*. Tech. rep. Accessed: 2025-05-18. NASA Jet Propulsion Laboratory, Mar. 2006. URL: https://www.jpl.nasa.gov/news/press_kits/mro-arrival.pdf.

[14] NASA. *Mars Reconnaissance Orbiter Mechanisms*. https://web.archive.org/web/20221202111942/https://mars.nasa.gov/mro/mission/spacecraft/parts/mechanisms/. Accessed: 2025-05-18.

[15] NASA. *Mars Reconnaissance Orbiter Science Instruments*. URL: https://science.nasa.gov/mission/mars-reconnaissance-orbiter/science-instruments/.

[16] NASA. *Thermal Systems*. Accessed: 2025-05-09. 2015. URL: https://web.archive.org/web/20150905185258/http://mars.nasa.gov/mro/mission/spacecraft/parts/thermal/.

[17] Northrop Grumman Systems Corporation. *Cryocoolers: Space Missions Made Possible*. https://www.northropgrumman.com/high-efficiency-cryocoolers. 2019.

[18] M O'Donnell and J Smithrick. "Nickel Hydrogen Batteries—An Overview". In: *NASA Lewis Research Center: Cleveland, OH, USA* (1995), p. 13.

[19] Lavagna Michéle Roberta. “SSEO-Attitude/orbit determination Control”. In: *Politecnico di Milano* (2025).

[20] RocketLab. “ST-16RT2 Datasheet STAR TRACKER High-Performance Star Tracker”. In: (2013).

[21] Newspace Systems. *Libra Reaction Wheels*. 2024. URL: https://www.newspacesystems.com/wp-content/uploads/2024/07/Reaction-Wheel-Datasheet-A4-9-1.pdf.

[22] Jim Taylor, Dennis K Lee, and Shervin Shambayati. “Mars reconnaissance orbiter”. In: *Deep Space Communications* (2016), pp. 193–250.

[23] Richard W. Zurek and Suzanne E. Smrekar. “An overview of the Mars Reconnaissance Orbiter (MRO) science mission”. In: *Journal of Geophysical Research: Planets* 112.E5 (2007). DOI: https://doi.org/10.1029/2006JE002701. eprint: https://agupubs.onlinelibrary.wiley.com/doi/pdf/10.1029/2006JE002701. URL: https://agupubs.onlinelibrary.wiley.com/doi/abs/10.1029/2006JE002701.

MRO Reverse Engineering Study

Assignment #7

Team 21

P. Code	Surname	Name
10724393	Chini	Filippo
10721870	Mazzitti	Riccardo
10682521	De Gennaro	Antonio
10764250	Bianco	Emanuele
10668777	Matteotti	Luca
10810285	Basci	Matteo Maria
11076681	Kazenas	Mantas

Space System Engineering and Operations

Prof: M. Lavagna

L. Bianchi, M. Bussolino

M.Sc Space Engineering
A.Y. 2024-2025

Change log	
Issue	*Comments*
1	First release

Contents

1 Command & Data-handling Systems **1**
1.1 **Space Flight Computers:** . . . 1
1.1.1 **RAD750 processor:** . . . 1
1.1.2 **Flight Software:** . . . 1
1.1.3 **C&DH Module Interface Card:** . . . 1
1.2 **Solid State Recorder:** . . . 2

2 Sizing **2**
2.1 Data budget breakdown table . . . 3

List of Acronyms	
Acronym	*Full Name*
C&DH	Command & Data-handling system
TMTC	Telecom & Telemetry System
PS	Propulsion System
ADCS	Attitude Determination & Control System
RW	Reaction Wheels
HGA	High Gain Antenna
TCS	Thermal Control System
EPS	Electrical Power System
OBDH	On-Board Data Handling
SFC	Space Flight Computer
IMU	Inertial Measurement Unit
LMSS	Lockeheed Martin Space Systems
CMCI	Command and Data Handling Module Interface Cards
SRAM	Static Random Access Memory
MCM	Multi-Chip Module
SSR	Solid State Recorder
FS	File System

1 Command & Data-handling Systems

Command & Data-handling systems (C&DH) has several crucial tasks and is essentially the "brains" of the orbiter. The key parts of this system are:

1.1 Space Flight Computers:

The MRO spacecraft is equipped with two redundant onboard computers—known as Side A and Side B, each forming a Command and Data Handling Subsystem (C&DH). These computers continuously synchronize their state and sensor data. Typically, one computer operates actively, while the other remains as a cold backup, capable of booting within tens of seconds.[5]

1.1.1 RAD750 processor:

The Mars Reconnaissance Orbiter (MRO) employs a space-qualified processor within its Space Flight Computer (SFC), utilizing the RAD750, a radiation-hardened variant of the PowerPC 750 or G3 processor. This 133 MHz processor, considered fast by space standards, contains 10.4 million transistors and operates on a custom-built motherboard specifically designed for space applications [6].
The RAD750 processor provides processing power of up to 46 million instructions per second (MIPS) (4% level 1 cache miss rate), the RAD750 efficiently supports the science and engineering instruments, along with the spacecraft's subsystems. Additionally, the Space Flight Computer has access to two gigabits of DRAM to store engineering status and health telemetry [2]. The processor's design prioritizes reduced power consumption, lower weight, and cost efficiency, achieving processing speeds up to 48 MIPS[4]. It is integrated into the CompactPCI Space Flight Computer, occupying three rack units [2].

1.1.2 Flight Software:

The Flight Software is an integral component of the Space Flight Computer (SFC), comprising numerous applications operating atop the VxWorks operating system, which provides extensive fault protection protocols and monitoring. A notable example of such an application is Fault Protection, designed to continuously monitor spacecraft systems for a broad spectrum of issues, automatically resolving them when feasible, and otherwise ensuring spacecraft safety. Additionally, higher-level commanding, image processing, and supplementary fault protection functions are delivered by instrument-specific software running on the SFC. Developed in ANSI C for the VxWorks environment, the SFC flight software is provided by Lockheed Martin Space Systems (LMSS), the spacecraft manufacturer, and leverages LMSS system services for fundamental operations, including uplink commanding, downlink data transmission, and interfacing with instrument hardware [1].

1.1.3 C&DH Module Interface Card:

Each space flight computer have one redundant Command and Data Handling Module Interface Cards (CMCI) that stores 2 Mbit image of the flight software. This images is utilized during the reboot sequence if the spacecraft enters safe mode and autonomously identifies that it needs to reboot. Such active redundancy is implemented to protect the essential flight data stored in the file system. Every CMIC is equipped with a Static Random Access Memory (SRAM) Multi-Chip Module (MCM), and each MCM stores two File System (FS) images on separate SRAM dies as seen in figure 1 [5]

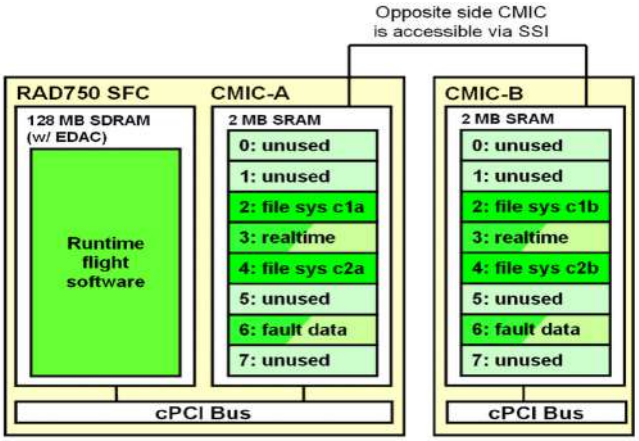

Figure 1: CMCI Structure [5]

1.2 Solid State Recorder:

The Solid State Recorder (SSR) is the primary onboard storage device for science instrument data collected by the spacecraft. It consists of an array of over 700 memory chips, each providing 256 megabits of storage capacity, for a total initial capacity of 160 Gigabits. This capacity, however, becomes limited when considering that a single high-resolution image from instruments like HiRISE can require up to 28 Gigabits.
To efficiently manage storage, the SSR is divided into two partitions: one designated for raw data and another for processed data. Raw instrument data initially stored in the raw data partition undergoes editing and formatting by the flight computer. Once formatted into packets, the processed data is stored in the second partition, ready for transmission to Earth. As data is downlinked, it is subsequently overwritten with new science data. At the end of the mission's operational life, the SSR's total effective science data storage capacity is expected to be around 100 Gigabits across both partitions.[6]
The computer also has available 128 megabytes of high-speed, random-access memory.[4]

2 Sizing

In the following table the data budget breakdown is presented. It includes the computations of the data volume required for the nominal operational mode and it encompasses the following subsystems: attitude sensors, ADCS, PS, TMTC, TCS, EPS, fault analysis subsystem, OBDH and other system devices. The table includes all the parameters that generate data whose status is required to be known for the success of the mission, that can be measured together with the number of values of each parameter, the data type along with the bit size, the sampling frequency and the data rate, which has been computed by multiplying the number of values, the bit size and the sampling frequency. The total data rate is represented by the sum of all the singular data rates, to which an margin of 400% is applied. In order to compute the total data volume it's necessary to multiply this value by the recording time, but since no information about it was found, this wasn't done during the calculations. The most critical element of the sizing is the processing of the gyro rate, due to the high frequency required in order to control the correct functioning of the gyroscopes, since the maneuvers that they need to do are really fast. This parameter takes up to 46.96% of the total datarate (without margins). It was decided that each component that measures physical quantities such as pressure, temperature, current and voltage didn't require a great precision, in order to reduce the total data volume, so an integer data type was chosen while for the sensors and actuators control a floating data type was

assumed due to the high complexity of their application. Some parameters were assumed as a boolean data type, which represents a binary condition (on/off), such as the valves and the sun presence sensors. A rather critical value to size was the runtime kernel, due to its multiple scopes and tasks, and it was decided to size it as a float32 type with a 100 Hz sampling frequency. Lastly, a float64 data type was assumed for 3 elements: ephemeris and orbit propagation and fault correction; all these parameters needed a very high accuracy, so this type of data was necessary, even though it requires a lot of data.
In this sizing, the payloads weren't considered because an accurate method to compute their data dimensions couldn't be found. In the real mission, the majority of the data volume is taken by these parameters, since the images they obtain are really heavy and require a lot of volume to be stored, in particular HiRise due to its capacity of taking high-definition pictures. This explains the difference between the memory size of the computer of the real mission (160 Gb [3]) and the value computed with this sizing, which otherwise would have been inexplicable.

2.1 Data budget breakdown table

Parameter name	n.	data type	bit size	frequency [Hz]	datarate [bps]
Attitude Sensor Processing					
Star tracker output	8	float32	32	10	2560
Sun presence sensor output	16	bool	1	1	16
Rate Gyro	4	float32	32	100	12800
IMU Current	1	sint16	16	1	16
IMU Voltage	1	sint16	16	1	16
IMU Temperature	1	sint16	16	0.5	8
Attitude Determination and Control					
Quaternion Estimation	4	float32	32	10	1280
Angular Rates Estimation	3	float32	32	10	960
Error Determination	2	float32	32	10	640
Thruster Control	8	float32	32	2	512
Reaction Wheel Control	4	float32	32	2	256
RW Saturation Flag	4	bool	1	1	4
Ephemeris Propagation	1	float64	64	1	64
Orbit Propagation	1	float64	64	1	64
Gimbals	3	float32	32	event based	-
PS					
Valves	10	bool	1	event based	-
Tank Pressure	4	uint16	16	0.5	32
Tank Temperature	4	sint16	16	0.5	32
Main Engines Control	6	float32	32	2	384
Secondary Engines Control	6	float32	32	10	1920
Engines Pressure	20	uint16	16	0.5	160
Engines Temperature	20	sint16	16	0.5	160
Fault Analysis					
Fault Detection (watchdog)	1	bool	1	1	1
Fault Correction	1	float64	64	5	320
Safe Mode Activation	1	bool	1	1	1
TMTC					
Command Processing (uplink)	2	float32	32	10	640

Parameter name	n.	data type	bit size	frequency [Hz]	datarate [bps]
Telemetry Processing (downlink)	2	float32	32	10	640
TCS					
Thermal Control	2	float32	32	1	64
EPS					
Battery Voltage	2	sint16	16	1	32
Battery Current	1	sint16	16	1	16
Battery Temperature	2	sint16	16	0.5	16
PCDU Temperature	2	sint16	16	0.5	16
Bus Voltage	1	sint16	16	1	16
Solar Arrays Current	20	sint16	16	1	320
System					
I/O Device Handlers	1	bool	1	1	1
Runtime Kernel	1	float32	32	100	3200
Simple Autonomy	1	bool	1	1	1
OBDH					
OBC temperature	1	sint16	16	0.5	8
OBC Voltage	1	sint16	16	1	16
OBC Current	1	sint16	16	1	16
Boot Count	1	uint16	16	1	16
Boot Cause	1	uint16	16	1	16
Stored Packet Count	1	uint16	16	1	16
TOTAL					27256
MARGINS 400%					109024
TOTAL + MARGINS					136280

References

[1] J. F. Bell III et al. "Mars Reconnaissance Orbiter Mars Color Imager (MARCI): Instrument description, calibration, and performance". In: *Journal of Geophysical Research: Planets* 114.E8 (2009). DOI: https://doi.org/10.1029/2008JE003315. eprint: https://agupubs.onlinelibrary.wiley.com/doi/pdf/10.1029/2008JE003315. URL: https://agupubs.onlinelibrary.wiley.com/doi/abs/10.1029/2008JE003315.

[2] Corelis Inc. *BAE Systems Success Story*. Accessed: 2025-05-31. 2005. URL: https://www.corelis.com/successstoriesdownload/BAE.pdf.

[3] NASA. *Mars Reconnaissance Orbiter - Command and Data Handling*. Accessed via Internet Archive on May 31, 2025. 2015. URL: https://web.archive.org/web/20150905201127/http://mars.nasa.gov/mro/mission/spacecraft/parts/command/.

[4] NASA Jet Propulsion Laboratory. *Mars Reconnaissance Orbiter Arrival Press Kit*. Accessed: 2025-05-31. Mar. 2006. URL: https://www.jpl.nasa.gov/news/press_kits/mro-arrival.pdf.

[5] NASA Jet Propulsion Laboratory. *MRO Spaceflight Computer Side Swap Anomalies*. Accessed: 2025-05-31. Dec. 2008. URL: https://llis.nasa.gov/lesson/2041.

[6] Ramon P. De Paula. "Mars Reconnaissance Orbiter Mission". In: *54th International Astronautical Congress of the International Astronautical Federation, the International Academy of Astronautics, and the International Institute of Space Law*. DOI: 10.2514/6.IAC-03-Q.3.a.01. eprint: https://arc.aiaa.org/doi/pdf/10.2514/6.IAC-03-Q.3.a.01. URL: https://arc.aiaa.org/doi/abs/10.2514/6.IAC-03-Q.3.a.01.

MRO Reverse Engineering Study

Assignment #8

Team 21

P. Code	Surname	Name
10724393	Chini	Filippo
10721870	Mazzitti	Riccardo
10682521	De Gennaro	Antonio
10764250	Bianco	Emanuele
10668777	Matteotti	Luca
10810285	Basci	Matteo Maria
11076681	Kazenas	Mantas

Space System Engineering and Operations

Prof: M. Lavagna

L. Bianchi, M. Bussolino

M.Sc Space Engineering
A.Y. 2024-2025

Change log	
Issue	*Comments*
1	First release

Contents

1 Structural design **1**
1.1 Materials 1

2 Configurations **2**
2.1 Launch Vehicle and Configuration 2
2.2 Cruise 2
2.3 Mars Orbit Insertion and Aerobraking 2
2.4 Science operations 2

3 Pointing Mechanisms **3**

4 Spacecraft Structure and Components **3**
4.1 External Structure 3
4.2 Internal Components 3

5 Subsystem mass budget **4**

1 Structural design

Since MRO main objective is to study Mars surface and atmosphere during science phase, nadir pointing is of paramount importance and is one of the main structure design drivers for the payloads, that are cameras and radars. This is evident in figure 1:

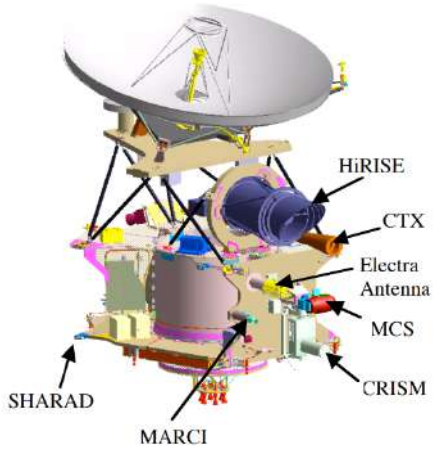

Figure 1: Payload configuration[1]

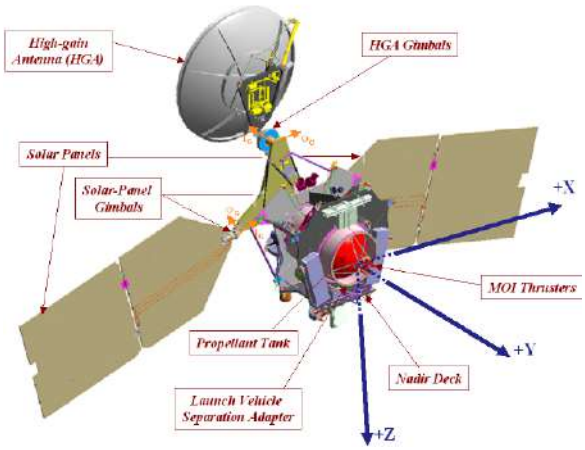

Figure 2: Deployed configuration

Another driver for the structure design, and also for the material selection, is the aerobraking phase, since the stagnation flow during this phase increases the temperature of the spacecraft to very high values.
In order to satisfy these drivers and also to bear mechanical stresses and loads, the primary structure, which is a prism with an hexagonal surface, that grants symmetry and compactness, has to protect the most thermally sensible components and subsystems from external heat fluxes, not only during the aerobraking phase but also during launch, and also provide solid attachments for payloads. The secondary structure is attached to the primary one to ensure overall structural integrity and its purpose is to provide dedicated support to single subsystems, such as thermal blankets for the payloads. An important component of the secondary structure, and one of the appendages of MRO together with the HGA, are the solar panels, which shall bear extreme heat fluxes during aerobraking phase, a factor that constrains their size. Their surface shall be large enough to avoid too high temperatures in localized points and specific materials are required to endure these temperatures. MRO has also a tertiary structure, composed mainly by cables, pipes and the gimbals that move the appendages (solar panels and HGA). They're designed for very specific applications such as controlling appendages or ensure the correct functioning of the electric and propulsion system.

1.1 Materials

In order to find a compromise between enduring big mechanical stresses due to the harsh space environment and having a light weight structure, the material assumed for the main body shell of MRO is Aluminum, that is famous for its high strength with respect to its weight and its low cost. More specifically, the main structure is composed of carbon composite panels bonded to an aluminum honeycomb core [3]. The solar arrays are made of five distinct layers: two composite facesheets, a solar cell layer, an aluminum honeycomb core and a Kapton layer. The central propellant tank is made of titanium and contributes to the spacecraft's structural integrity due to titanium's strength and resistance to corrosion.

2 Configurations

2.1 Launch Vehicle and Configuration

The mission was planed to use an Atlas V 401 rocket[5] seen in figure 3 . The rocket consists of two-stages for the launch. Upper stage named Centaur is capable of performing multiple burns, enabling the rocket to have better precision and control that is required to correctly target Mars. Atlas V has a 4.2 m wide payload and a length of 12.2 m. Here in Fig.4, can be seen the folded spacecraft configuration that has to fit in the payload fairing of the launcher. [1]

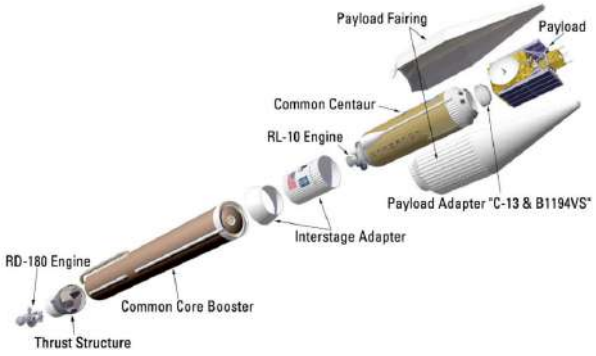

Figure 3: Atlas V breakdown[1]

2.2 Cruise

The spacecraft deployed the solar arrays after that MRO detached the Centaur. The high gain antenna was also deployed to point Earth. [Fig. 5]

2.3 Mars Orbit Insertion and Aerobraking

The configuration here is really similar to the one of the Cruise, except for the angle of high gain antenna, that during aerobraking has to balance the torque given by the solar arrays. [Fig.6]

2.4 Science operations

In science operations the spacecraft shall point instruments to Mars for imaging while pointing the solar arrays and high gain antenna towards, respectively, to the Sun and Earth. [Fig.7]

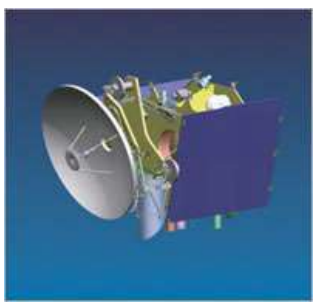

Figure 4: Launch[4]

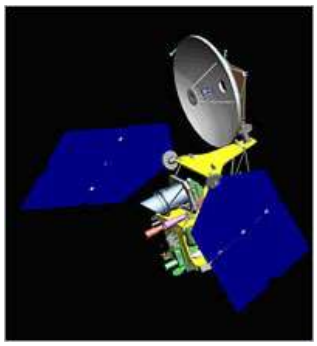

Figure 5: Cruise[4]

Figure 6: MOI-ABX[4]

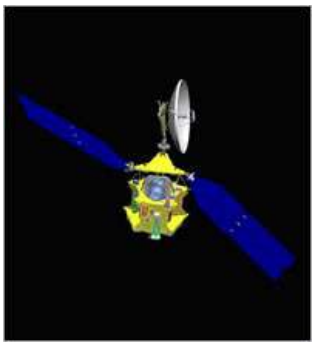

Figure 7: Science[4]

3 Pointing Mechanisms

To fulfill its diverse science goals, the (MRO) employs a combination of gimbaled mounts and precise spacecraft orientation systems to direct its instruments. The CRISM instrument is mounted on a two-axis gimbal, allowing it to track fixed locations on the Martian surface as the spacecraft moves overhead. It can scan up to $\pm 60^\circ$ along the flight path, enabling targeted imaging and atmospheric correction by observing the same location from multiple angles. The MCS features an articulating pedestal that lets its two telescopes rotate independently of the spacecraft. This allows for continuous atmospheric profiling from the surface to space, and periodic calibration using deep space views. Other instruments, such as HiRISE and CTX, rely on spacecraft body-pointing rather than internal gimbals. MRO uses reaction wheels for fine control and hydrazine thrusters for larger maneuvers and momentum dumping. This setup is able to target the desired object with an high accuracy, which is required for high-resolution and stereo imaging. These mechanisms provide MRO with the precision needed to achieve the requirements for this mission.

4 Spacecraft Structure and Components

4.1 External Structure

This table takes as reference axes the ones in Fig.2.

Components	**Description**
CRISM, MCS, MARCI, ELECTRA, HiRISE, CTX	First constraint for the satellite design since they are required to look to Mars for imaging and communication → satellite needs to perform nadir pointing → located in the +Z face
Solar Arrays	2 solar arrays to guarantee symmetry → choose by design the faces +-Y
High Gain Antenna	Antenna diameter: 3m. → while deployed put in the -Y face to increase the cross section area during aerobraking and also to balance the momentum around the X axis given by the solar array during this process
Orbit insertion thrusters	8 engines located symmetrically with respect to the center of +Y face to perform orbit insertion
Secondary and control thrusters	12 coupled thruster used to perform attitude control and orbit correction maneuver → located all over the main body
Low Gain Antennas	Placed behind the high gain antenna
Thermal blanket	Cover all the main body for thermal constraints
SHARAD	Antenna put in the +Y face, along the -Z axis
ONC	Camera put on the +Z axis

4.2 Internal Components

The internal elements placement in the spacecraft is listed in priority/need order.

- **Propellant Tank**: One of the mission drivers is pointing control, so the propellant sloshing is a critical issue in the positioning of propellant tanks, since the available propellant mass at the beginning of PSP is around 300kg. For this reason, the propellant tanks are positionally

constrained near the CoM, to stabilize the CoM along the Y and X coordinates, while the Z coordinate lowers during the mission. This position ensures an optimal trade-off between the aforementioned sloshing, propellant storage at the operational range temperature, fit compatibility, length of pipes to the combustion chamber.

- **Pressurant Tank**: placed above Tanks, along -Z and slightly -Y with respect to the CoM, beside the upper hemispherical caps of the propellant tank, to leverage the non-diagonal coefficients in the inertia matrix to reduce the difference between pitch axis and roll axis
- **4 Reaction Wheels**: Skewed configuration → placed above the Tanks, and evenly distributed in the internal part of the face -Z, as close as possible to the CoM, to minimise concentrated torques and also not to interfere with payload observations
- **IMU**: placed -Z relative to the CoM for the same reason of RWs.
- **2 Star Trackers**: placed on -X and +X each. This is because for most of the mission lifetime the solar panels are oriented with their normal direction to the Sun direction, shadowing Star Trackers from sunlit, and also to avoid at most the presence of Mars in the FOV over the entire orbit.
- **3 Cryocoolers**: those of CRISM and CTX in the internal part close to +Z face, near the respective payload lens, and that of HiRISE in proximity of -Y face, to cool down the lenses.
- **Battery Pack**: placed slightly -Y, +Z relative to the CoM, close to the Tanks, for proximity to payloads, to minimise the cable length, and so the cable losses due to Joule effect. This ensures optimal heat-up of the envelopes and cooling-down of the payloads' lens. Moreover, this placement is strategical for non-complex routings and also to reduce the difference between the pitch and roll axis. Since -Y face is covered in MLI blankets, the battery pack is properly insulated from solar radiation, so solar radiation merely affects the temperature of the pack.
- **Heaters**: While the actual number of heaters is not well documented in the literature, at least there is one heater in the internal part of the face -Z because it shall heat up the reaction wheels during eclipse phase, and another one in the internal part of +Z face and +Y with respect to the CoM, to ensure proper thermal control of the payloads located on the main body's +Z face and not to exchange heat with the batteries, which have a tight temperature range. Moreover, the distribution of heaters in the spacecraft is critical to the active thermal control of the propellant temperature because it helps to maintain the propellant above the freezing point during the eclipse phase, even though the titanium tank is set in insulating layers.

5 Subsystem mass budget

The structure subsystem mass budget is presented in table 1:

Shell	Gimbals (3)	Cables	**TOTAL**
491 kg	45 kg	50 kg	586 kg

Table 1: Structure subsystem mass budget

For the shell mass, an assumption based on the total dry (50% of m_{dry}) mass was made, with MRO dry mass being 981 kg [2]. For the cables an assumption of 5% of the dry mass was made, while for the gimbals the value is taken from [6], without accounting for the drive motors and adding the gimbals for solar arrays.

References

[1] James E. Graf et al. "The Mars Reconnaissance Orbiter Mission". In: *Acta Astronautica* 57.2 (2005). Infinite Possibilities Global Realities, Selected Proceedings of the 55th International Astronautical Federation Congress, Vancouver, Canada, 4-8 October 2004, pp. 566–578. ISSN: 0094-5765. DOI: https://doi.org/10.1016/j.actaastro.2005.03.043. URL: https://www.sciencedirect.com/science/article/pii/S0094576505000780.

[2] Martin D Johnston et al. "The Mars Reconnaissance Orbiter mission: From launch to the primary science orbit". In: *2007 IEEE Aerospace Conference*. IEEE. 2007, pp. 1–19.

[3] JPL. *Orbiter's Skeleton*. 2005. URL: https://www.jpl.nasa.gov/images/pia07211-orbiters-skeleton/.

[4] NASA. *Mars Reconnaissance Orbiter: Spacecraft Configuration*. https://web.archive.org/web/20150905092756/http://mars.nasa.gov/mro/mission/spacecraft/config/. Accessed: 2025-06-08. 2015. URL: https://web.archive.org/web/20150905092756/http://mars.nasa.gov/mro/mission/spacecraft/config/.

[5] NASA Science. *Chapter 14: Launch*. Accessed: 2025-06-05. 2025. URL: https://science.nasa.gov/learn/basics-of-space-flight/chapter14-1/.

[6] Jim Taylor, Dennis K Lee, and Shervin Shambayati. "Mars reconnaissance orbiter". In: *Deep Space Communications* (2016), pp. 193–250.

MRO Reverse Engineering Study

Assignment #8b

Team 21

P. Code	Surname	Name
10724393	Chini	Filippo
10721870	Mazzitti	Riccardo
10682521	De Gennaro	Antonio
10764250	Bianco	Emanuele
10668777	Matteotti	Luca
10810285	Basci	Matteo Maria
11076681	Kazenas	Mantas

Space System Engineering and Operations

Prof: M. Lavagna

L. Bianchi, M. Bussolino

M.Sc Space Engineering
A.Y. 2024-2025

Change log	
Issue	*Comments*
1	First release

Contents

1 Tables of mass budget **1**

2 Comments on mass budget **1**

1 Tables of mass budget

-	**Mass without margin** [kg]	**Margin adopted** [%]	**Mass with margin** [kg]
PS	127.53	-	-
TTMTC	207.7	-	-
ADCS	39.65	-	-
TCS	24.9	-	-
EPS	186.39	-	-
OBDH	11.1	-	-
Structure	541	-	-
Payload	125.4	-	-
Dry mass	981	-	-
Fuel mass	1199	-	-
Wet mass	2180	-	-
Launchable mass	3893	-	-

Table 1: Mass budget from literature

-	**Mass without margin** [kg]	**Margin adopted** [%]	**Mass with margin** [kg]
PS	52.5	10	57.75
TTMTC	207.7	-	207.7
ADCS	39.65	-	39.65
TCS	24.9	-	24.9
EPS	127.9	25-10-5	141.02
OBDH	11.1	-	30
Structure	541	-	541
Payload	125.4	-	125.4
Dry mass sum	1171.39	20	1401.71
Fuel mass	969	5.5	1022.3
Wet mass	2424	-	2424
Launchable mass	3893	-	3893

Table 2: Mass budget from reports

2 Comments on mass budget

Regarding the PS and the EPS, their data from literature couldn't be found, so, using the tables present in the lecture slides regarding the margins, they were estimated as 13% and 19% of the dry mass, respectively. On the other hand, their data from our reports were found by adding together the values of their components, such as tanks or solar cells, that we computed. The margins used for the EPS include 25% for the solar cells to include harnessing for solar panels, 5% for the batteries and 10% for the solar panels gimbals. The last two values are the Design Maturity Mass Margins; since the batteries are commonly used in space missions, a 5% margin should suffice, while for the gimbals a greater margin was deemed necessary.
Many of the subsystems masses couldn't be found in literature, so they were assumed based on similar missions, such as the OBDH, which was taken from Mars Odyssey [1], or deduced from datasheets of various components, such as ADCS, Payloads and TTMTC. For this reason, their values are the same

for both tables.
The structure subsystem was computed as a percentage of the dry mass value taken from literature, as stated in the structure subsystem paragraph.
The main differences between the literature and report values of dry, fuel and wet masses are due to the margins applied, that usually represent the worst case scenario. It's important to note that the dry mass value in table 1 is taken from literature and doesn't match the sum of the various subsystems. This is because of the assumptions made, which have been previously stated. The value of the wet mass without margin has been computed has the sum of the dry and fuel masses with margins.
The last remark that has to be done is regarding the launchable mass. The value in the tables corresponds to the highest mass that the launcher of MRO, Atlas V 401 , has ever launched in space [2], since an exact value for the maximum mass that Atlas V can carry couldn't be found.

References

[1] NASA JPL. *Mars Odyssey*. URL: `https://science.nasa.gov/mission/odyssey/`.

[2] National Aeronautics and Space Administration, Jet Propulsion Laboratory (NASA/JPL-Caltech). *Mars Science Laboratory Landing Press Kit*. Press Kit. Mass: 8,463 lb (3,893 kg) total at launch, consisting of 1,982-lb (899-kg) rover; 5,293-lb (2,401-kg) Entry, Descent and Landing system. Pasadena, CA: NASA Jet Propulsion Laboratory, July 2012. URL: `https://www.jpl.nasa.gov/news/press_kits/MSLLanding.pdf`.